Seasonal distribution and drivers of surface fine particulate matter and organic aerosol over the Indo-Gangetic Plain

Caterina Mogno[1], Paul I. Palmer[1,2], Christoph Knote[3], Fei Yao[1], and Timothy J. Wallington[4]

[1]School of GeoSciences, University of Edinburgh, Edinburgh, UK
[2]National Centre for Earth Observation, University of Edinburgh, Edinburgh, UK
[3]Model-Based Environmental Exposure Science (MBEES), Faculty of Medicine, University of Augsburg, Germany
[4]Research & Advanced Engineering, Ford Motor Company, Dearborn, MI, 48121-2053, USA

Correspondence: Caterina Mogno (c.mogno@ed.ac.uk)

Abstract.

The Indo-Gangetic Plain (IGP) is home to 9% of the global population and is responsible for a large fraction of agricultural crop production in Pakistan, India, and Bangladesh. Levels of fine particulate matter (mean diameter <2.5 microns, $PM_{2.5}$) across the IGP often exceed human health recommendations, making cities across the IGP among the most polluted in the world. Seasonal changes in the physical environment over the IGP are dominated by the large-scale South Asian monsoon system that dictates the timing of agricultural planting and harvesting. We use the WRF-Chem model to study the seasonal anthropogenic, pyrogenic, and biogenic influences on fine particulate matter and its constituent organic aerosol (OA) over the IGP that straddles Pakistan, India, and Bangladesh during 2017/2018. We find that surface air quality during pre-monsoon (March—May) and monsoon (June—September) seasons is better than during post-monsoon (October—December) and winter (January—February) seasons, but all seasonal mean values of $PM_{2.5}$ still exceed the recommended levels, so that air pollution is a year-round problem. Anthropogenic emissions influence the magnitude and distribution of $PM_{2.5}$ and OA throughout the year, especially over urban sites, while pyrogenic emissions result in localized contributions over the central and upper parts of IGP in all non-monsoonal seasons, with the highest impact during post-monsoon seasons that correspond to the post-harvest season in the agricultural calendar. Biogenic emissions play an important role in the magnitude and distribution of $PM_{2.5}$ and OA during the monsoon season, and shows a substantial contribution to secondary OA (SOA) particularly over the lower IGP. We find that the OA contribution to $PM_{2.5}$ is significant in all four seasons (17-30%), with primary OA generally representing the larger fractional contribution. We find that the volatility distribution of SOA is driven mainly by the mean total OA loading and the washout of aerosols and gas-phase aerosol precursors that result in SOA being less volatile during the pre-monsoon and monsoon season than during the post-monsoon and winter seasons.

1 Introduction

The Indo-Gangetic Plain (IGP), including parts of Pakistan, India and Bangladesh (Figure 1), is one of the most populous and polluted areas in the world. **It is home to $\sim$ 700 million people (9% of the global population (Bangladesh Bureau of Statistics, 2011; Indian National Commission on Population, 2020; Pakistan Bureau of Statistics, 2017)) and to the**
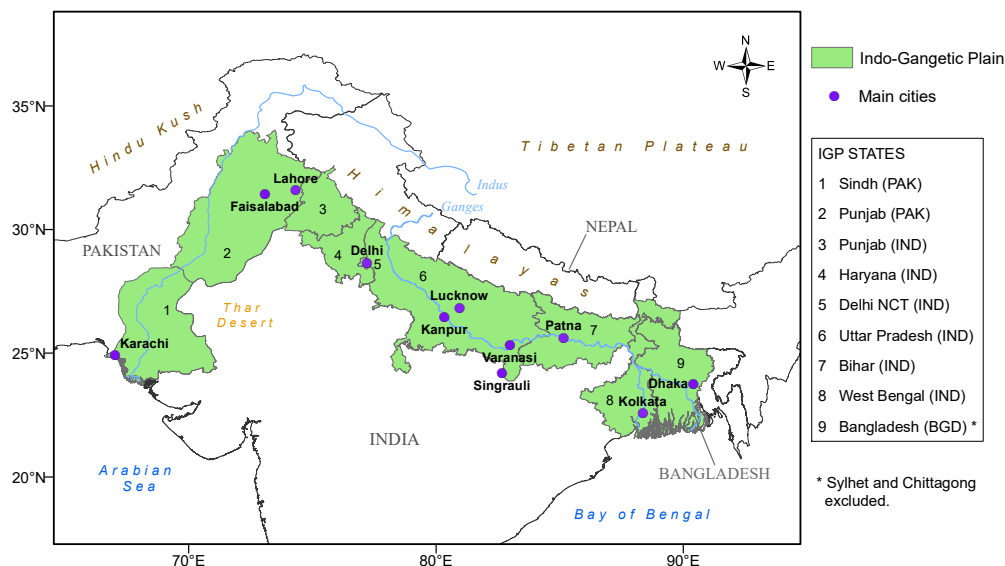
Figure 1. Geographical and administrative features of the Indo-Gangetic Plain (IGP), including Pakistan, India, and Bangladesh. Numbers denote individual IGP states and purple dots denote the main cities.

associated sources of anthropogenic air pollution, which are distributed proportionally to population, with hotspots
25 over cities of various sizes from megacities of more than 10 million people, e.g. Karachi, Lahore, Delhi, Kolkata, and
Dhaka, to smaller cities of a few million inhabitants, e.g. Faisalabad, Patna, Kanpur, Lucknow, and Varanasi (DESA,
2018). It has been estimated that there would be a potential gain in life expectancy in the IGP of approximately 4-6 years
if levels of $PM_{2.5}$ were reduced to standards set by the World Health Organisation (Greenstone et al., 2020; WHO, 2016).
The unique geography of the IGP and broader scale meteorological drivers, coupled with the regional diversity of seasonal
30 pollutant emission sources makes this region one of the most challenging places to study the controls of its air pollution and
the consequent impact on human health. Here, we use the WRF-Chem regional atmospheric chemistry and transport model to
describe the seasonal patterns of surface organic aerosol and $PM_{2.5}$ and to help disentangle the role of anthropogenic, pyrogenic
and biogenic emissions on their surface patterns across the IGP.

The importance of the IGP lies in the fertility of its soils formed from alluvium that is deposited across the Indus and Ganges
35 basins by the Indus and Ganges rivers. These rivers originate in the Himalaya mountains and the Tibetan Plateau. The Indus and
Ganges basins benefit also from precipitation from the seasonal monsoon. The monsoon timing also defines the main seasons
over the IGP (India Meteorological Department): the pre-monsoon season runs from March to May, the monsoon season is

from June to September, the post-monsoon season is from October to December, and winter occurs in January and February. The Indian states across the IGP (e.g. Punjab, Haryana, and Uttar Pradesh) represent the vast majority of nationwide wheat

40 and rice production. Rice and wheat are planted in May and November and harvested in October-November and April-May respectively, following the rice–wheat cropping cycle. The IGP is also an important producer of sugarcane, cultivated mainly in the Indus Valley in Pakistan and in the Indian state of Uttar-Pradesh. The two main seasons for planting are in September-October and February-March, followed by harvesting during the winter and pre-monsoon months, respectively. Crop residues left from harvesting, e.g. husk, bran, straw, are generally burned in open fires. Traditionally, these residues were ploughed back

45 into the soil to maintain fertility and stability, but the sheer scale of current production precludes these practices in time for a second growing season (Chauhan et al., 2012; Ahmed et al., 2015). Open burning of these residues across the IGP, particularly during the post-monsoon season, is a large source of gaseous and particulate pollution that has implications for regional air quality and human health (Vadrevu et al., 2011; Jethva et al., 2019; Sembhi et al., 2020). Residential biofuel combustion also plays an important role for air quality (Conibear et al., 2020; Agarwala and Chandel, 2020).

50 The high population density and intense human activity over the IGP result in anthropogenic emissions being a major source of regional surface air pollution (Begum et al., 2013; Guttikunda and Jawahar, 2014; Shahid et al., 2015; Venkataraman et al., 2018). Residential energy consumption represents a major contribution to anthropogenic emissions with a large fraction of the rural and urban population using solid fuel for cooking (Conibear et al., 2018). Emissions from land transportation, particularly in cities, also represents a significant contribution to anthropogenic emissions (Begum et al., 2013; Guttikunda et al., 2014;

55 Mallik and Lal, 2014). Intense agriculture over the IGP is associated with large emissions of ammonia, an aerosol precursor, from urea fertilizer application, as well as from post-harvest burning as described above (Kuttippurath et al., 2020; Wang et al., 2020). Vegetation cover over the IGP consists mainly of croplands (Stibig et al., 2007; Gumma et al., 2019), which have lower isoprene emissions than trees (Hardacre et al., 2013). Consequently, biogenic emissions over the IGP are lower compared to other parts of South Asia (Guenther et al., 2006; Stavrakou et al., 2014).

60 Regional dispersion of air pollution over the IGP is dominated on a seasonal timescale by the monsoon system, influenced by the high mountain ranges of Hindu Kush and Himalayas that lie to the northwest to northeast of the IGP. Agricultural planting and harvesting (and associated burning) are determined by the timing of the monsoon when the majority of the annual rainfall falls. Consequently, observed variations of $PM_{2.5}$ reflect large-scale variations in meteorology and the seasonal variations in anthropogenic, biogenic, and pyrogenic emissions (Jethva et al., 2005; Lelieveld et al., 2018; Schnell et al., 2018).

65 A growing body of regional models have been used to study the relationship between emissions, meteorology, and $PM_{2.5}$ over India (Kumar et al., 2015b; Bran and Srivastava, 2017; Kulkarni et al., 2020; Ojha et al., 2020), and to estimate the health impacts of outdoor exposure to $PM_{2.5}$ (Ghude et al., 2016; Conibear et al., 2018; David et al., 2019). Many studies have focused on post-monsoon biomass burning episodes and on air pollution during the winter season over the upper-central Indian part of the IGP (Guttikunda and Gurjar, 2012; Ram et al., 2012; Pant et al., 2015; Kumar et al., 2015a; Jethva et al., 2018; Singh

70 et al., 2018; Krishna et al., 2019; Mhawish et al., 2020). But of course the IGP also includes parts of Pakistan and Bangladesh that remain poorly studied even though they are connected via atmospheric transport. With only a few exceptions, these studies have focused on total $PM_{2.5}$ although there is evidence that single aerosol components play a major role in $PM_{2.5}$ composition

over the IGP (Gani et al. (2019) and Singh et al. (2018) and references therein). Measurements have shown that organic aerosol (OA), originating from anthropogenic, pyrogenic, and biogenic emissions, constitute a significant fraction (20-35%) of $PM_{2.5}$ across the IGP especially during post-monsoon and winter seasons (Ram et al., 2008; Alam et al., 2014; Rajput et al., 2014; Behera and Sharma, 2015; Sharma et al., 2016). OA exists as a complex mixture, comprising of thousands of individual organic compounds, and it is made up of primary OA (POA), emitted directly to the atmosphere, and of secondary OA (SOA) formed by the condensation of organic vapours as they become progressively less volatile through oxidation (Seinfeld and Pandis, 2016; Donahue et al., 2006). Changes in OA volatility is key for the formation of SOA, and it is particularly sensitive to temperature, ambient concentration of OA, and nitrogen oxide levels (Shrivastava et al., 2017). We take advantage of the Volatility Basis Set (VBS) model, which helps to describe succinctly the evolving volatility of OA through oxidative chemistry in the atmosphere (Donahue et al., 2006, 2012; Chuang and Donahue, 2016), described below. This method has been used successfully in a range of modelling studies (Lane et al., 2008b; Bergström et al., 2012; Ahmadov et al., 2012; Zhang et al., 2013; Zhao et al., 2016).

We use the WRF-Chem regional atmospheric chemistry model to characterise the seasonal and spatial distributions and composition of $PM_{2.5}$ and OA in light of synoptic meteorology and emission drivers over three sub-regions of the IGP, including relevant parts of Pakistan and Bangladesh. We use a 1-D VBS model to describe the evolution of OA and its influence on $PM_{2.5}$, described in section 2. In section 2, we also describe the *in situ* and satellite measurements we use to evaluate our model. In section 3, we describe the seasonal meteorology over the IGP, the seasonal distributions and composition of $PM_{2.5}$ and OA, and the seasonal distribution of SOA volatility. In section 3 we also use a perturbative approach to understand the sensitivity of $PM_{2.5}$ constituent distributions to changes in anthropogenic, pyrogenic and biogenic emissions and to seasonal changes in the atmospheric environment. We conclude our study in section 4.

2 Data and Methods

Here, we describe the WRF-Chem model that we use to understand the influence of anthropogenic, pyrogenic, and biogenic emissions on the atmospheric distribution of $PM_{2.5}$ and OA over the IGP.

2.1 Weather Research and Forecasting model coupled with Chemistry

We use v.3.9.1.1 of the the Weather Research and Forecasting (WRF) model coupled with Chemistry (WRF-Chem) (Grell et al., 2005) to describe the emissions and atmospheric chemistry and transport associated with gas and aerosol phase compounds over the IGP during 2017 and 2018. WRF uses the Advanced Research WRF (ARW) dynamical solver to solve the fully compressible, non-hydrostatic Euler equations that describe atmospheric flow. These calculations are coupled with atmospheric chemistry so that that our $PM_{2.5}$ and OA calculations are consistent with the meteorology.

Our study domain is defined as 17°–40° N and 64°–97° E, encompassing the IGP at a horizontal spatial resolution of 20 km and using 33 vertical levels that span from the surface to 50 hPa ($\simeq$19 km). **For the description of terrain data for the domain (land use and soil categories) we use MODIS IGPB 21-category data at 30 arc-seconds resolution ($\sim$ 1 km) (Friedl et al., 2010).** To define our initial conditions and lateral boundary conditions, and for nudging (Newtonian relaxation),
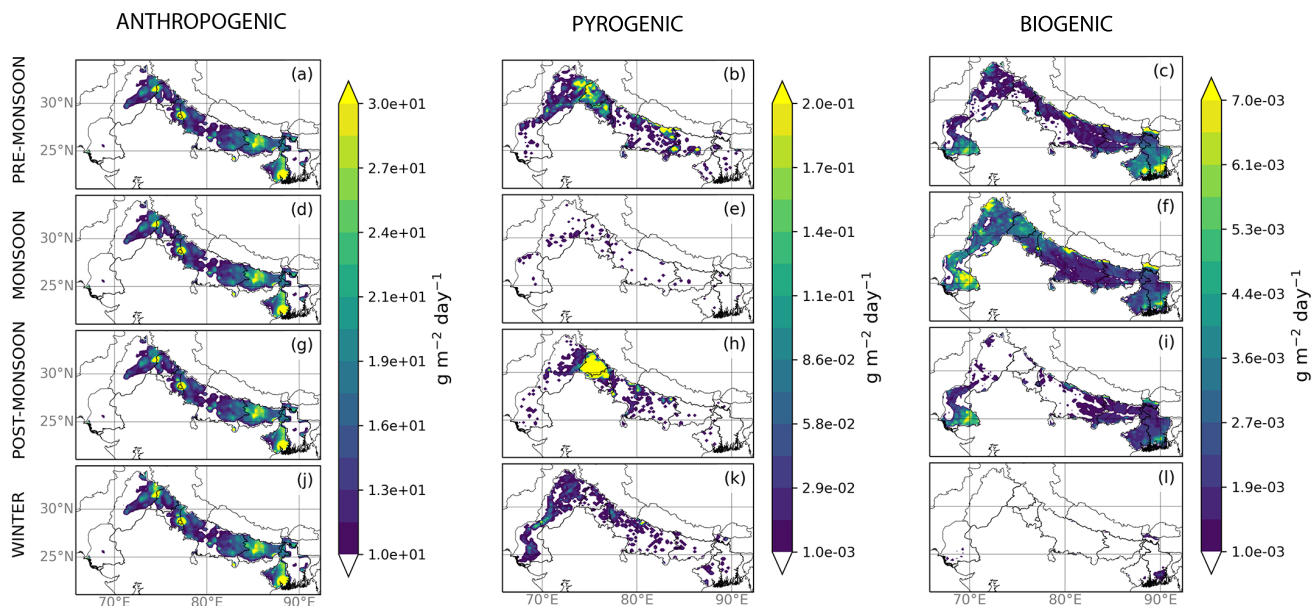
Figure 2. Seasonal mean daily emissions over the IGP (g m^{-2} day^{-1}) of (left) column) anthropogenic, (middle column) biomass burning, and (right column) biogenic (isoprene) emissions. Anthropogenic emissions from EDGAR-HTAP and fire emissions from FINN. Biogenic emissions are calculated online in WRF-Chem using MEGAN. **To determine total anthropogenic and pyrogenic emissions we sum across all emitted species, respectively, while for biogenic emissions we consider only isoprene.**

105   we use meteorological reanalyses from NCEP FNL Operational Model Global Tropospheric Analyses Data (National Centers for Environmental Prediction, National Weather Service, NOAA, U.S. Department of Commerce, 2015) at a spatial resolution of 0.25°×0.25° and at a temporal resolution of six hours. We use the nudging approach at all levels to prevent our calculations from deviating too far from observed meteorology. Table B1 provides more details about the meteorological processes we use in our calculations. Chemical initial conditions and lateral boundary conditions for each month are provided by six-hourly

110   CAM-CHEM global model data (Buchholz et al., 2019). We spin-up each simulation for a week before studying the model output to minimize the influence of the initial conditions.

     To describe gas-phase chemistry we use the Model for OZone And Related chemical Tracers, version 4 (MOZART-4) chemical mechanism (Emmons et al., 2010), including the extended treatment of volatile organic compound (VOC) chemistry (Knote et al., 2014). Photolysis rates are calculated by the Fast Tropospheric Ultraviolet–Visible (FTUV) module (Tie et al.,

115   2003).

     We use the Model for Simulating Aerosol Interactions and Chemistry (MOSAIC) to simulate aerosols chemistry (Zaveri et al., 2008), including aqueous-phase chemistry (Knote et al., 2014). MOSAIC describes aerosols using four sectional discrete size bins: 0.039—0.156μ m, 0.156—0.625μ m, 0.625—2.5μ m, 2.5–10μ m. The first three of these bins represent PM$_{2.5}$, while the largest one describes coarse particulate matter (PM$_{2.5-10}$). We use the 1-D VBS method to describe SOA for WRF-Chem

120   (Knote et al., 2015), based on previous studies (Lane et al., 2008b; Ahmadov et al., 2012). For each of the four aerosol size

bins in MOSAIC, the 1-D VBS implementation considers five volatility bins for semi-volatile organic compounds (SVOCs), described by effective saturation concentrations C^* of 10^{-4}, 1, 10, 100 and 10^3 $\mu g\ m^{-3}$ at 298 K. The $log_{10}C^* = -4$ volatility corresponds to an inert compound, and serves computationally as a loss of particle phase organics to avoid unrealistic volatile mixtures due to continuously aging of gas-phase SVOCs. Lumped anthropogenic, pyrogenic, and biogenic gas-phase aerosol precursors undergo continuous gas-phase oxidation and partition between the gas and aerosol phase using pseudo-ideal partitioning theory (Pankow, 1994). Partitioning between the gas and aerosol phase depends on total organic aerosol load and temperature. SOA yields are also dependent on NO_x levels, so SOA yields is calculated differently for low and high NO_x conditions, through a branching ratio (Lane et al., 2008a). We also include the SOA formation from glyoxal (Knote et al., 2014). Loss of SVOCs is from washout via convective and grid scale precipitation. Our chosen implementation of VBS only accounts for SVOCs, and assumes that POA is inert so that it contributes only to the aerosol mass. We do not include direct emissions of SVOCs or intermediate VOCs (IVOCs). This is a limitation of our current implementation given evidence that SVOC and IVOC vapours creates a considerable amount of regional SOA, and that POA emissions are semivolatile and undergo oxidation and should be also considered in describing SOA production (Robinson et al., 2007). To describe POA using the VBS approach we would require information about the volatility distribution of POA, but conventional inventories typically consider POA as non-volatile. **The 1-D version of the VBS model is unable to describe some aspects of SOA formation, including fragmentation and the increase in OA oxidation state, which are better described by the 2-D version of the model that tracks the oxygen-to-carbon ratio (O:C) in addition to organic mass (Donahue et al., 2012). Previous studies have shown that the 2-D VBS model improves model-measurement agreement in SOA (e.g., Zhao et al. (2016)) but has a significant associated computational burden when used in 3-D chemistry transport models.** Further details of this VBS implementation in WRF-Chem are described in (Knote et al., 2015) and references therein.

We use monthly anthropogenic emissions from Emission Database for Global Atmospheric Research with Task Force on Hemispheric Transport of Air Pollution (EDGAR-HTAP v2.2) for year 2010 (Janssens-Maenhout et al., 2015) as provided by the WRF-Chem community, which provides the total anthropogenic emissions and includes a NMVOC speciation according to the gas and aerosol chemistry scheme we use here (MOZART-MOSAIC). **Using an anthropogenic emission inventory for 2010 to describe atmospheric chemistry during 2017-2018 will inevitably introduce some biases in our model PM$_{2.5}$ estimates, particularly because our study domain includes regions with rapidly growing emissions. From 2010 to 2017, India has seen reductions in BC, OC, CO and NMVOC emissions from the residential sector owing to policies that have enabled a switch to cleaner residential fuels and energy sources. However India's growing economy had led to a rapid increase of NO_x and SO_2 emissions from the industrial sector($\sim +12\%$, $\sim +10\%$) and energy sector ($\sim +20\%$, $\sim +26\%$), and an increase in NO_x and NMVOC from on-road transportation ($\sim +50\%$, $\sim +27\%$). An increase in intensive agricultural practices over the Indian IGP has increased ammonia emissions NH_3 ($\sim +15\%$) (McDuffie et al., 2020). Errors in PM precursor gaseous emissions will impact our ability to describe air pollution for our study year, especially for individual components of secondary inorganic aerosols (nitrate, sulfate and ammonium) and SOA. It remains difficult to disentangle the impact of using outdated emission estimates from other sources of model error, e.g., meteorology, chemistry, land-use change, and model resolution.** For pyrogenic emissions, hourly biomass burning emissions are taken from the

Fire Inventory from NCAR (FINNv.15) inventory for year 2017/2018 (Wiedinmyer et al., 2011). **Pyrogenic emissions are apportioned between FINN and EDGAR-HTAP inventories. The FINNv1.5 inventory includes global estimates of trace gas and particle emissions from open burning of biomass, which includes wildfire, agricultural fires, and prescribed burning (Wiedinmyer et al., 2011). EDGAR-HTAPv2.2 is focused on anthropogenic emissions but excludes large-scale biomass burning (e.g. forest fires, peat fires), agricultural waste or field burning. Within its residential sector, emissions include small-scale combustion, including heating, lighting, cooking and solid waste disposal or incineration (Janssens-Maenhout et al., 2015).** Biogenic emissions are calculated online using the Model of Emissions of Gases and Aerosol from Nature (MEGAN, Guenther et al. (2006)).

Figure 2 shows the seasonal distributions of total anthropogenic, pyrogenic, and biogenic (predominately isoprene) emissions over the IGP. Total anthropogenic emissions have been calculated by summing the mass contribution from all the chemical species (gas and particle) specified in the inventory once preprocessed onto the model domain using the WRF-Chem tools for the community ACOM-NCAR. We converted gas emissions to mass units using the appropriate molar mass for each species. The same approach has been used to calculate fire emissions, while isoprene emissions are calculated online by MEGAN in the WRF-Chem model and then converted to mass units. Anthropogenic emissions generally dominate in all seasons (Figure 2a,d,g,j) with daily values ranging from 10^1 to 10^2g m^{-2} day^{-1}. The two largest localised regions of anthropogenic emissions are Delhi and Kolkata with emissions >100 g m^{-2} day^{-1}, followed by smaller indian cities, e.g. Patna, Varanasi, Kanpur and Lucknow (Figure 1). Just south of the border of Uttar-Pradesh, the Madhya Pradesh district of Singrauli hosts several large power plants. The Pakistani and Bangladeshi parts of the IGP generally have the lowest anthropogenic emissions, with the exception of Karachi in south Pakistan, the north Pakistani Punjab (the most populated part of Pakistan where Lahore and **Faisalabad** are located), and Dhaka in Bangladesh. Emissions from Karachi and Dhaka have lower per capita emissions than Indian cities of comparable size.

Fires have a strong seasonal cycle, peaking during pre-monsoon and post-monsoon seasons (Figure 2b,h), with emissions $\sim 10^{-1}$g m^{-2} day^{-1} mainly due to agricultural stubble burning. The post-monsoon harvesting season includes fire emissions rates that are three times higher compared to the pre-monsoon season (~ 0.3 g m^{-2} day^{-1} and ~ 0.9 g m^{-2} day^{-1}, respectively). Post-monsoon fires are almost exclusively located in the Indian Punjab, with the largest values at the border with Haryana state. Pre-monsoon fires are located around the border of Pakistani and Indian Punjab and upper Haryana. There are also some isolated fires in the eastern part of the IGP. During winter (Figure 2k), low fire activity is present in the Indus valley in Pakistan and mainly over Uttar-Pradesh from post-harvesting of sugarcane crop.

Biogenic emissions peak during pre-monsoon and monsoon seasons (Figure 2c,f), with values of 2×10^{-3}g m^{-2} day^{-1} and 1.5×10^{-2}g m^{-2} day^{-1}, respectively. The largest values are over Sindh in Pakistan, West Bengal, and Bangladesh. Land cover over the IGP is dominated by croplands, but state of Sindh includes coastal mangrove plantations, inlands riverine forests, irrigated plantations, and rangelands (**Ministry of Environment Government of Pakistan, 2009**). Moreover, West Bengal and Bangladesh emissions are mostly confined close to the coast, where forest land is present (Reddy et al., 2016). During these two seasons there are also isoprene emissions over Uttar Pradesh from forests in Pilibhit and Kheri, and from northeast Pakistan.

For computational expediency we have chosen a representative period of one month for each distinct season over the IGP. We define, based on the seasonal definition of the Indian Meteorological Department (India Meteorological Department), the pre-monsoon period as 18th April to 16th May 2017; the monsoon season as 3rd to 31st July 2017; the post monsoon season at 18th October to 16th November 2017; and finally winter as 8th January to 5th February 2018. The 2017/2018 year is close to the climatological mean state so our results are typical of this region rather than being influenced by significant circulation changes due to, for example, El Niño Southern Oscillation climate variations (Null, 2020).

For the purposes of reporting our results we divide the IGP into three sub-regions: the upper IGP that includes the Pakistani states of Sindh and Punjab and the Indian Punjab; the middle IGP that includes the Indian states of Haryana, Delhi NCT, and Uttar Pradesh; and the lower IGP that include the Indian state of Bihar and West Bengal and Bangladesh, excluding the states of Chittagong and Sylhet (Figure 1).

2.2   Determining the Sensitivity of $PM_{2.5}$ and OA to Changes in Precursor Emissions

We use a perturbative approach to determine the importance of different source sectors on $PM_{2.5}$ and OA, which takes into account the non-linear chemical environment. Alternatively, setting a particular emission source to zero would result in a significant non-linear response that is unique to the source, consequently precluding any meaningful comparison of the importance of a particular source to $PM_{2.5}$ and OA.

First, we run a base run for each season. We then, for each season, systematically perturb one emission source by +5% over the study domain for the central week of each season, keeping the other sources the same as the base run. **Finally, we calculate the sensitivity S_{ij} of species concentration to the changes in a given source of emissions as:**

$$S_{ij} = \frac{\Delta C_{ij}}{\Delta E} = \frac{\Delta C_{ij}}{E_{tot}^p - E_{tot}^b} = \frac{\sum_t (C_{ij,t}^p - C_{ij,t}^b)}{\sum_{ij,t,s} (E_{ij,t,s}^p - E_{ij,t,s}^b)}, \tag{1}$$

where ΔC_{ij} represents the concentration change of our target species ($PM_{2.5}$ and OA in this study) at grid point ij in response to an emission change ΔE summed over the IGP for a particular source. We perturb directly anthropogenic and fire emissions rates. Biogenic emissions are calculated online by scaling normalized emission rates by factors that describes changes in, for example, temperature, photosynthetic active radiation, leaf area index (LAI) (Guenther et al., 2006). We modify the WRF-Chem code to increment only isoprene emissions because our calculations suggest they account for almost all of biogenic emissions over the IGP, in agreement with other studies (Singh et al., 2011; Surl et al., 2018). ΔC_{ij} is calculated by summing over time the difference in concentrations at each grid cell ij of the perturbed run p $C_{ij,t}^p$ and the base run b $C_{ij,t}^b$. The change in concentration in each grid cell is therefore scaled by the same ΔE, allowing to consider local and non-local emission influences equally and to avoid singularities in grid cells where there is no net emission change. We use this scaling because it allows us to compare the sensitivity of atmospheric concentrations to different sources types. ΔE is calculated as the difference of total emissions within the IGP domain between the perturbed model run and the base model run for a given source type.

Total emissions across the IGP for the perturbed run E_{tot}^p and for the base run E_{tot}^b are calculated by summing emissions from all species for the length of the simulation and for all grid cells across the IGP. In more detail, emissions at

each grid point ij for species s between two consecutive model outputs at t and $t+1$ is calculated (for both the perturbed and base runs) by $E_{ij,t,s} = \epsilon_{ij,t,s}\Delta t A_{ij}$. $\epsilon_{ij,t,s}$ denotes the emission rate of species s at location ij and output time t, A_{ij} denotes the area of grid point ij, which in our calculations is constant at 400 km^2, and Δt corresponds to an interval of model output which in our calculation is 3 hours. To take into account the different spatial variability of emissions from different sources (Figure 2), we scale ΔE with the total number of grid cells within the IGP for which the emission difference is >0.001 g m^{-2} day^{-1}, corresponding approximately to cumulative emissions > 2.8 Mg for each grid cell in one week. This threshold corresponds to a lower limit for significant emissions rate across the area considered (Figure 2). We also neglect values of S_{ij} for which the change in the pollutant concentration C_{ij} <5% of mean pollutant seasonal concentration over the IGP (4 μg m^{-3} and 1 μg m^{-3} for PM$_{2.5}$ and total OA, respectively). Using this additional threshold allows us to isolate significant changes in concentrations due to direct changes in emissions, and remove smaller values due to model non-linearity. We report the sensitivity parameter S_{ij} with units of μg m^{-3} Gg^{-1}. In a policy-making context, our sensitivity parameter provides information about how to control atmospheric concentrations by changing different emission sources in order to obtain the highest air quality benefits from certain emission reductions.

2.3   Data Used for Model Evaluation

We use *in situ* measurements of PM$_{2.5}$, PM$_{10}$, CO, NO$_2$, O$_3$, and SO$_2$ from the Indian Central Pollution Control Board CPCB and PM$_{2.5}$ data collected atop the US Embassy in Pakistan and Bangladesh U.S. Department of State. We accessed these data from the OpenAQ Platform (OpenAQ). Appendix B describes an overview of the *in situ* data, our data cleaning approach, and evaluation metrics. Given the lack of continuous measurements of OA and its **components** POA and SOA over the IGP, we compare our model OA with measurements available from the literature. We also evaluate the model using satellite observations of aerosol optical depth (AOD) from the NASA Moderate Resolution Imaging Spectroradiometer (MODIS) instrument aboard the Terra and Aqua satellites, which have a local equatorial overpass time of 1030 and 1330, respectively. AODs are retrieved at 550 nm, corresponding to particle sizes of 0.1–2μm and comparable to the PM$_{2.5}$ size range. In particular, we use the MODIS Collection 6.1 Level 2 combined Dark Target and Deep Blue AOD product available on a 10 km spatial resolution (Levy et al., 2013).

Here we summarize the main results of our evaluation (detailed results are available in Appendix B). We report the normalized mean bias (NMB) and the Pearson correlation coefficient r, which we use to describe how well the model reproduces the observations. The model tends to overestimate surface PM$_{2.5}$ concentrations (0.004<NMB<0.4) especially during monsoon season (NMB=0.4) but it has skill in reproducing observed seasonal variations ($r > 0.62$) with the exception of the monsoon season ($r = 0.09$). **Poorer model performance during the monsoon period may be due to a number of compounding factors. In particular, it is challenging to reproduce observed atmospheric water vapour and precipitation over the Bay of Bengal, western coasts of India and the Himalayan foothills during summer months. Uncertainties in the representation of topography, insufficient mixing in the boundary layer, errors in moisture transport and simulation of surface moisture availability, soil temperature and an excessive water vapour flux from the ocean all contribute to model error**

(Kumar et al., 2012a). Previous studies have shown that monsoonal rainfall is not well described by regional models such as MM5 or WRF (Rakesh et al., 2009; Ratnam and Kumar, 2005). When we compare our WRF model simulation with MERRA-2 reanalysed meteorology (Gelaro et al., 2017) we find that precipitation rates have a negative model bias of $\simeq 80\%$ over the IGP, similarly to what Conibear et al. (2018) obtained with a similar model set-up.

For PM_{10}, the model tends to underestimate the observation in all seasons (NMB up to -0.25) except in premonsoon season (NMB=0.15) and has poorer skill in reproducing observed PM_{10} variations compared to $PM_{2.5}$ ($r \leq 0.69$), especially during winter and pre-monsoon season. **We generally find poorer model agreement with gas-phase pollutants, including a positive model bias and comparatively poor correlations with observations of NO_2, SO_2 O_3 (Table A3). We attribute this to multiple sources of error. Given the coarse spatial and temporal resolution our model (20 km$\times$20 km spatial, 3 hour temporal), we expect our model to be affected by non-negligible representation error due to the CPCB network sites often being located near to roadsides or in dense urban areas where the model will struggle to reproduce. This source of error preferentially affects reactive trace gases that react on timescales with transport across individual model grid cells. Previous studies have reported similar model limitations (Fountoukis et al., 2013; Paolella et al., 2018; Kuik et al., 2016; Tan et al., 2015; Sirithian and Thepanondh, 2016; Balasubramanian et al., 2020). Data for Pakistan are not available for our modelling study period (2017/2018) so we instead use data from 2019 for the monsoon and post-monsoon seasons and data from 2020 for the winter and pre-monsoon seasons, which represents an additional source of error. Previous studies show that regional modelling over south Asia tends to overestimate satellite column observations of NO_2 by 10–50% over the Indo-Gangetic Plain, the bias peaking as high at 90% during winter months (Kumar et al., 2012b), and up to +131% when compared to ground-based observations over densely populated urban regions (Karambelas et al., 2018). These differences have been attributed mainly to errors in NO_x emission inventories over densely populated areas, uncertainties in seasonal variations of emissions, absence of diurnal and vertical profiles of anthropogenic emissions(Kumar et al., 2012b; Karambelas et al., 2018), and underestimation of precipitation rate that will reduce the loss of soluble trace gases Kumar et al. (2012a). Similarly, previous regional model studies of IGP region have tended to over-predict concentrations of SO_2, with NMB>3.5 (Conibear et al., 2018; Kota et al., 2018). We attribute our positive model bias of SO_2 to using an outdated emission inventory that does not take into account the beginning of a shift from coal to gas-based power plants (Sharma and Khare, 2017). Urbanisation has been shown to affect the diurnal spatial distribution of surface ozone (Li et al. (2014) and references therein), and also the magnitude and location of anthropogenic emissions of NO_x and VOCs that subsequently affect surface ozone photochemistry (Zhang et al., 2004; Ghude et al., 2013). Finally, some fraction of the overestimation of surface ozone is linked to our use of the MOZART chemical mechanism that has been previously reported to have a positive model bias over south Asia compared to other mechanisms (Sharma et al., 2017). Collectively, these model limitations associated with describing reactive trace gases will impact our ability to model particulate matter, especially secondary components over urban areas across the IGP.**

For OA, the model reproduces the order-of-magnitude seasonal trends (Table B4) but additional measurements are needed to robustly assess model performance. Table B5 shows that WRF-Chem AOD agree with spatial distributions of MODIS AODs with r typically > 0.5 with the exception of the monsoon season (r=0.35). **Poor model skill during the monsoon season may**

reflect difficulties in retrieving AOD during extensive seasonal cloud coverage and simulating atmospheric aerosols, as highlighted earlier in this section.. The model tends to overestimate MODIS AOD during pre-monsoon (NMB=0.33, 0.26 for Terra and Aqua satellites) and slightly underestimate AOD in the other seasons (NMB ranges from -0.06 to -0.19).

3 Results

First, we summarise the seasonal meteorology over the IGP, which influences the physical and chemical environments that determine $PM_{2.5}$ and OA. We then report seasonal distributions of surface $PM_{2.5}$ and the corresponding constituent aerosol composition. Finally, we investigate the seasonal influence of POA and SOA on $PM_{2.5}$ and the volatility of the surface SOA across the IGP. In describing the seasonal distribution of $PM_{2.5}$, OA, POA and SOA we highlight the influence of anthropogenic, pyrogenic, and biogenic emissions and synoptic meteorology in shaping these patterns.

For the purpose of describing $PM_{2.5}$ and OA we begin our narrative with the post-monsoon season and finish with the monsoon season, reflecting the central importance of the monsoon system on atmospheric chemistry over the IGP. However, in the corresponding figures we retain the chronological order of events in a calendar year.

3.1 Seasonal Meteorological Drivers

Figure A1 shows model seasonal mean values for planetary boundary layer height (PBLH, m), surface relative humidity (RH, %), surface temperature (°C), mean daily rainfall (mm day^{-1}), and 10 m wind (m s^{-1}) over the IGP. Given that PBLH and RH show a diurnal cycle with high variance we report nighttime and daytime values for these variables.

During the pre-monsoon season, mean surface temperatures are higher than 30°C. Mean PBLH ranges from 1000 m up to 4500 m at daytime, with the highest values are over Pakistan and central IGP, and is almost an order of magnitude smaller during nighttime (120 m up to 400 m). Seasonal mean winds are typically 3 m s^{-1}, southward from the northern mountain chain of Hindu Kush and the Himalayas, and stronger northward from the coast, allowing pollutants to be transported mainly in the inland. Air is much more humid over the lowest part of the IGP (>60%). Rainfall follows similar patterns of RH, limited to Bangladesh with values below ∼3 mm day^{-1}.

During the monsoon season, the dominant feature is the monsoon itself. This manifests most obviously in increased rainfall, which increases the washout of hydrophillic pollutants, mainly in the central and lower part of the IGP, with mean daily rainfall values of 3-7 mm day^{-1} with localized regions of rainfall in excess of 15 mm day^{-1}, and wind speeds in excess of 6 m s^{-1} north-northeastward. Values of RH are >50% almost everywhere over the IGP, and relatively low values for the PBLH allow a well mixed chemical environment, with smaller day to night variation compared to pre-monsoon (1000-3000 m day, 500-1200 m night). Mean temperatures are similar to those during the pre-monsoon, with the most prominent increase over northern Pakistan (>35 °C).

The post-monsoon season is characterized by cooler temperatures than the previous two seasons with mean values of ∼23°C, much lower values for PBLH (below 2000 m during day and ∼200 m during night), and weaker wind speeds (< 1 m s^{-1} with no predominant direction, a combination of factors that results in pollution stagnation. With the exception of Bangladesh and
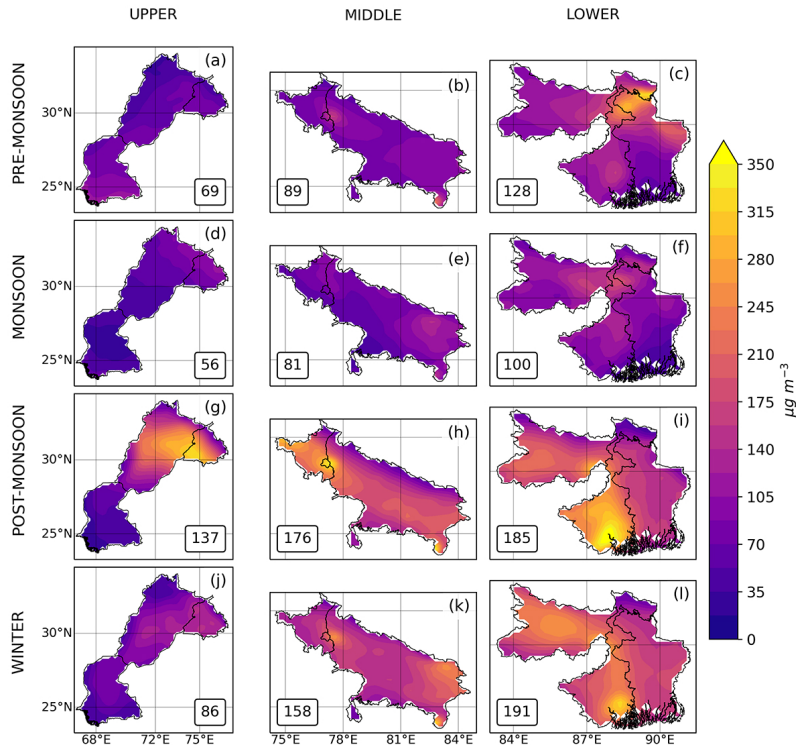
Figure 3. Seasonal mean spatial distributions of PM$_{2.5}$ (μg m^{-3}) over the upper, middle and lower IGP. The numbers inset of pre-monsoon (a–c), monsoon (d–f), post-monsoon (g–i), and winter (l–n) seasons denote the regional mean PM$_{2.5}$ value.

325 the Indian states that are adjacent to the Bay of Bengal, rainfall is almost absent from the IGP. Nevertheless, air continues to be humid with the distribution and values of RH similar to the monsoon season, with values of up to 80% over the central and lower IGP, environmental conditions that favour water significantly contributing to PM mass without washout from rain.

  During winter, mean temperature further drops to ~15°C with cooler temperatures over regions adjacent to the northern mountain chains. PBLH values are at their daily annual minimum (<~1000 m) and its night values are similar to post-monsoon

330 (<~200 m). Winds speeds are typically <12 m s^{-1} with a net west-east gradient from the upper IGP to the lower IGP, which transports pollutants towards Bihar, West Bengal and Bangladesh, and with a north-south gradient over the Indus Basin that transports pollution from northern Pakistan to the coast. Daily rainfall is below 3 mm day^{-1} anywhere across the IGP, but as for post-monsoon, RH remains high over the central and lower IGP (>40% daytime, 70% during nighttime).

3.2 Seasonal Distributions of Surface PM$_{2.5}$

335 Figure 3 shows seasonal variations of surface PM$_{2.5}$ across the upper, middle, and lower IGP. Generally, we find the highest values of surface PM$_{2.5}$, up to 350 μg m^{-3}, during post-monsoon and winter seasons that are associated with lower PBLH allowing large anthropogenic emissions to accumulate in the boundary layer without ventilation from strong winds. From this
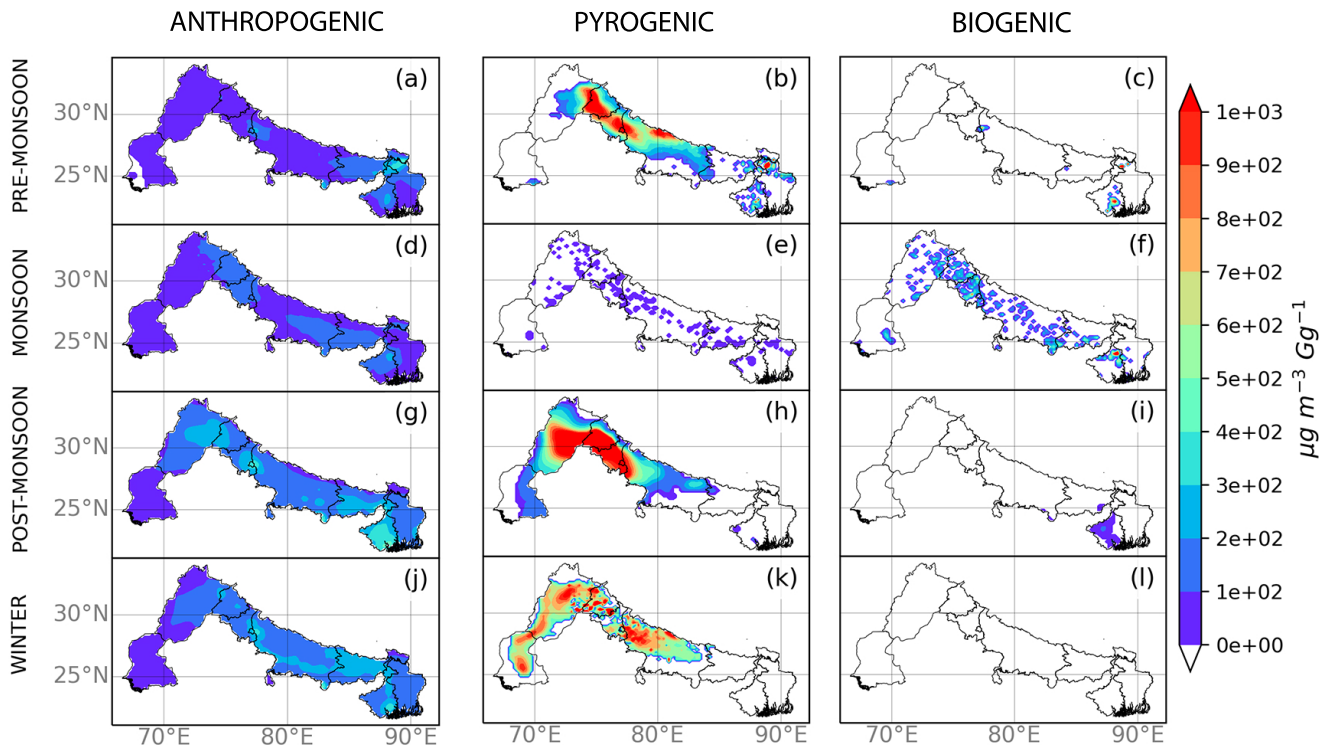
Figure 4. Seasonal sensitivity of PM$_{2.5}$ concentrations to changes in (left column) anthropogenic, (middle column) pyrogenic, and (right column) biogenic emissions (μ g m^{-3}Gg^{-1}). The calculation is described in the main text. Regions marked as white denote where sensitivity corresponds to PM$_{2.5}$ concentrations below the set threshold of 4 μg m^{-3}.

section we begin **our** narrative from the post-monsoon season and finish with the monsoon season, but retain the figure panels in chronological order for a particular calendar year. Our seasonal distributions of PM$_{2.5}$ are similar to recent studies (Shahid et al., 2015; Ojha et al., 2020; Mhawish et al., 2020) although we report higher PM$_{2.5}$ concentrations especially over the lower IGP. **Compared to these studies, our model also takes into account water content in PM$_{2.5}$ mass in addition to dry PM$_{2.5}$ mass through aqueous phase chemistry. Our results shows that water content in PM$_{2.5}$ is substantial, especially over the lower IGP where water makes up to 42% of total PM$_{2.5}$ mass (see later in this section). This helps to explain our comparatively high PM$_{2.5}$ estimates.**

During the post-monsoon season (Figure 3 (g–i)), the mean values of surface PM$_{2.5}$ in the upper, middle, and lower IGP are 137 μg m^{-3}, 176 μg m^{-3}, and 185 μg m^{-3}, respectively. On a local scale, Kolkata and its surroundings in the lower IGP experience the worst air quality with mean PM$_{2.5}$ values in excess of 300 μg m^{-3}, closely followed by Delhi NCT, the border region between Indian and Pakistani Punjab, and Singrauli at the southern border of middle IGP ($\sim$300 μg m^{-3}). The best air quality is found in the Pakistani state of Sindh with PM$_{2.5}$ concentrations below 75 μg m^{-3}. Biomass burning in the Indian Punjab plays a key role in shaping the distribution of PM$_{2.5}$ during this season. Figure 4h shows that fire emissions have the

largest impact on PM$_{2.5}$ concentrations across the Indian and Pakistani Punjab region, Haryana and Delhi NCT (sensitivities of up to $> 10^3$ μg m^{-3} Gg^{-1}). **The impact of post-monsoon biomass burning emissions extends to the central part of the middle IGP over Uttar-Pradesh, where sensitivity of PM$_{2.5}$ to pyrogenic emissions (up to 6×10^2 μg m^{-3} Gg^{-1}) is higher than anthopogenic emissions (up to 4×10^2 μg m^{-3} Gg^{-1}).**

355   The sensitivity of PM$_{2.5}$ to changes in biogenic emissions (Figure 4i) have non-negligible values ($< 2 \times 10^2$ μg m^{-3} Gg^{-1}) only over part of West Bengal in the lower IGP.

During the winter season (Figure 3(j–l)), wind patterns transport pollutants from the upper IGP to the lower IGP, resulting in west-east gradient in seasonal mean PM$_{2.5}$ concentrations . The mean PM$_{2.5}$ value in the lower IGP is 191 μg m^{-3}, the highest mean seasonal value for the IGP. The highest PM$_{2.5}$ concentrations are reached in Kolkata ($>$300 μg m^{-3}), and in the Bihar

360   state, with a local peak in Patna ($>$220 μg m^{-3}) known as the 'Bihar pollution pool' (Kumar et al., 2018). In the middle IGP, mean PM$_{2.5}$ concentrations are 18 μg m^{-3} lower than post-monsoon levels, with east Delhi and Singauli remaining the largest hotspots of the region ($>$220 μg m^{-3}). The upper IGP experiences the lowest seasonal PM$_{2.5}$ concentration (86 μg m^{-3}), lower than half the value in the lower IGP, with concentrations decreasing from the Punjab to the Sindth coast. Anthropogenic emissions dominate the distribution of PM$_{2.5}$ during winter over the lower IGP (sensitivity up to 4×10^2 μg m^{-3} Gg^{-1}, Figure

365   4j), with the highest sensitivities over cities Kolkata, Singrauli. The influence of biomass burning is is significant over the the Indus basin, stretching until Uttar Pradesh (sensitivity up to 10^3 μg m^{-3} Gg^{-1}, Figure 4k), while biogenic emissions do not show a significant influence during this season (Figure 4l).

During the pre-monsoon season (Figure 3 a–c), air quality begins to improve due to higher PBLHs and stronger winds (Figure A1) that help to disperse pollutants. Mean PM$_{2.5}$ concentrations are similar over the upper and middle IGP with values lower

370   than 90 μg m^{-3}. Higher concentrations remain in the lower IGP (128 μg m^{-3}) due to the accumulation of pollutants from the winds blowing from the Bay of Bengal to the slopes of the Himalayas over North Bangladesh. **High aerosol loading over the lower IGP during the premonsoon season is also influenced by biomass burning from Northeast India and Myanmar-Laos, which are partially included in our model domain.** PM$_{2.5}$ values over the upper part of the middle IGP (Figure3 b) show some influence from biomass burning (Figure 4 b). We find that anthropogenic emissions are most important over

375   the lower IGP and localized region in the central IGP (Figure 4 a). PM$_{2.5}$ concentrations in Delhi NCT are jointly influenced by biomass burning and anthropogenic sources. Biogenic sources only have a significant impact over localized regions in the lower and middle IGP (Figure 4(c)).

Generally, the onset of the monsoon results in better air quality across the IGP due to higher rainfall rates, which increases wet deposition of aerosols, and higher PBLHs that improve the physical dispersal of surface emissions. Mean values of PM$_{2.5}$

380   are $\leq$100 μg m^{-3} across the IGP. The largest values of PM$_{2.5}$ are over the lower IGP (up to 170 μg m^{-3}). **We find that PM$_{2.5}$ is sensitive to biogenic emissions over localized regions across the IGP, where PM$_{2.5}$ can be more sensitive to changes in biogenic emissions than changes in anthropogenic emissions ($\sim$200-500 μg m^{-3}) and $<$200 μg m^{-3}, respectively).** Fires play only a small role in PM$_{2.5}$ during this season.
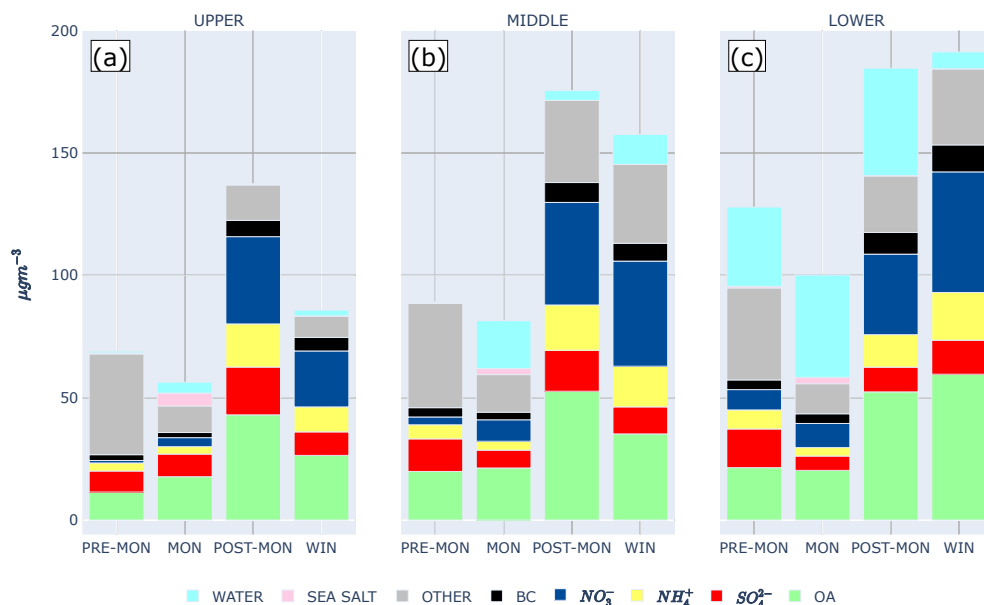
Figure 5. Seasonal mean PM$_{2.5}$ composition from the WRF-Chem model across the IGP: (a) upper, (b), middle, and (c) lower IGP. The constituents include sea salt (sum of sodium (Na) and chloride (Cl)), NH_4^+, SO_4^{2-}, NO_3^-, the sum of the remaining inorganic compounds (OTHER), total OA, BC, and liquid water.

Surface PM$_{2.5}$ composition

385   **Figure 5 shows the modelled composition of PM$_{2.5}$ across the IGP.** Generally, we find more variability between seasons than across different parts of the IGP, except for the water contribution to PM$_{2.5}$ mass. The results we report for the chemical composition and seasonal trends of PM$_{2.5}$ are broadly consistent with chemical characterisation studies over the region (Chowdhury et al., 2007; Bhowmik et al., 2020). **As discussed in Section 2.3, model limitations in reproducing precursor trace gases will affect our ability to model secondary components of particulate matter. When comparing the model**

390   **with recent field observations of PM$_1$ over Delhi during postmonsoon and winter (Gani et al., 2019; Gunthe et al., 2021; Patel et al., 2021), corresponding to two of our study seasons, we find that the model generally underestimates PM$_1$ (57-161 μg m^{-3} observed, 17-22 μg m^{-3} simulated) although we acknowledge that the model configuration we use is not ideal to model sub-micron PM due to our use of four sectional size bins. The model overestimates the contribution of PM$_1$ from nitrate (6-11% observed, 11-13% simulated), but underestimates the contributions from sulfate (7-9%**

395   **observed, 2% simulated) and organics (54-68% observed, 16-18% simulated).**

    Inorganic species (secondary inorganic aerosol of sulfate, nitrate and ammonium and other inorganic aerosol) dominate the chemical composition by mass of PM$_{2.5}$, representing between 30–80% of total PM$_{2.5}$ for each season across the IGP.

The mean seasonal mass of total inorganics across the IGP is 54–70 μg m^{-3} during the pre-monsoon season, 27–35 μg m^{-3} during the monsoon season, 79–111 μg m^{-3} during the post-monsoon season, and 51–114 μg m^{-3} during winter. The largest inorganic aerosol values are found during the post-monsoon and winter seasons due to nitrate from fossil fuel combustion and from residential and energy use. We find a similar but relatively muted seasonal variation for black carbon with mass values between 2–11 μg m^{-3}. Sea salt transported from the coasts during the monsoon season adds 3–5 μg m^{-3} (3–9%) to PM$_{2.5}$ across the IGP.

The water contribution to PM$_{2.5}$ is substantial over the lower IGP during pre-monsoon, monsoon, and post-monsoon seasons, with mass contribution of 32–44 μg m^{-3} (25–42%), while during winter it accounts for 6 μg m^{-3} (3.5%). For the middle IGP, water is a non-negligible fraction of PM$_{2.5}$ mainly during monsoon (20 μg m^{-3}, 24%) and winter (12 μg m^{-3}, 8%) seasons, while for the upper IGP the highest values of water mass are found during only the monsoon season (4 μg m^{-3}, 8%). The seasonal variation of water content reflects RH distribuions, which above values of 60–70% allows PM hydrophilic components (e.g., nitrate, sulfate, sea salt) to uptake water via deliquescence.

The sum of primary and secondary OA contributes by mass between 17% and 31% of PM$_{2.5}$ across the IGP, with contributions from POA and SOA varying with season. During the pre-monsoon season, OA contributes 11–21 μg m^{-3} to PM$_{2.5}$, representing 17–22% of the total mass. A similar mass contribution is found during the monsoon season (18–21 μg m^{-3}) but with higher percentage contribution to PM$_{2.5}$ (20–31%). The percentage mass contribution of OA to PM$_{2.5}$ is similar during the post-monsoon (28–31%, 43–52 μg m^{-3}) and winter (22–31%, 26–60 μg m^{-3}), with higher mass contribution during post-monsoon for the middle and lower IGP and during the winter season for the lower IGP. Our results for modeled PM$_{2.5}$ composition confirm the significance of OA contribution to fine particulate matter, and we analyse in more detail OA and its components in the next sections.

3.3 Seasonal Distribution of Surface OA
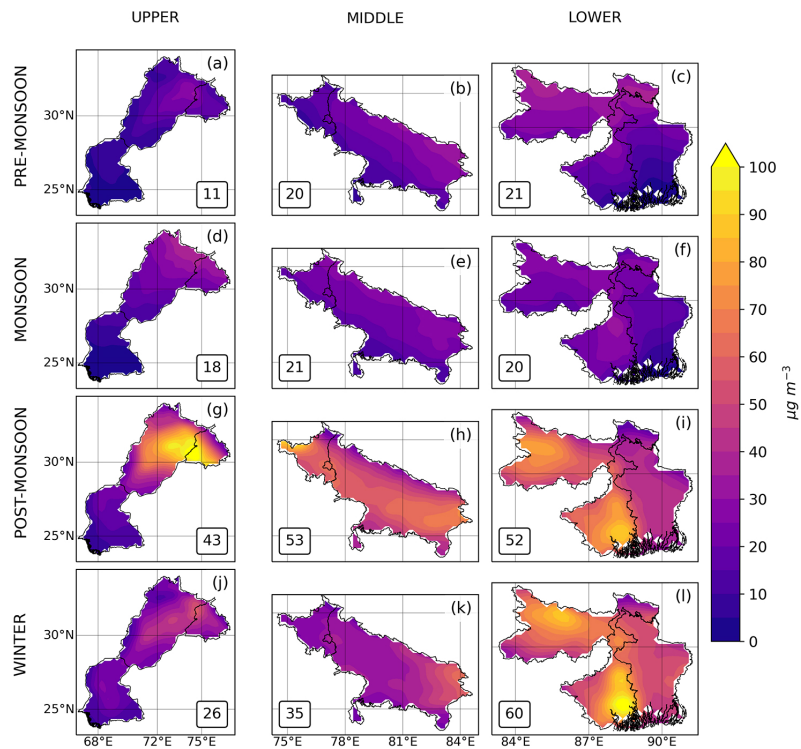
Figure 6. Seasonal mean distributions of total OA over the upper, middle and lower IGP. The numbers inset of pre-monsoon (a–c), monsoon (d–f), post-monsoon (g–i), and winter (l–n) seasons denote the regional mean total OA value.
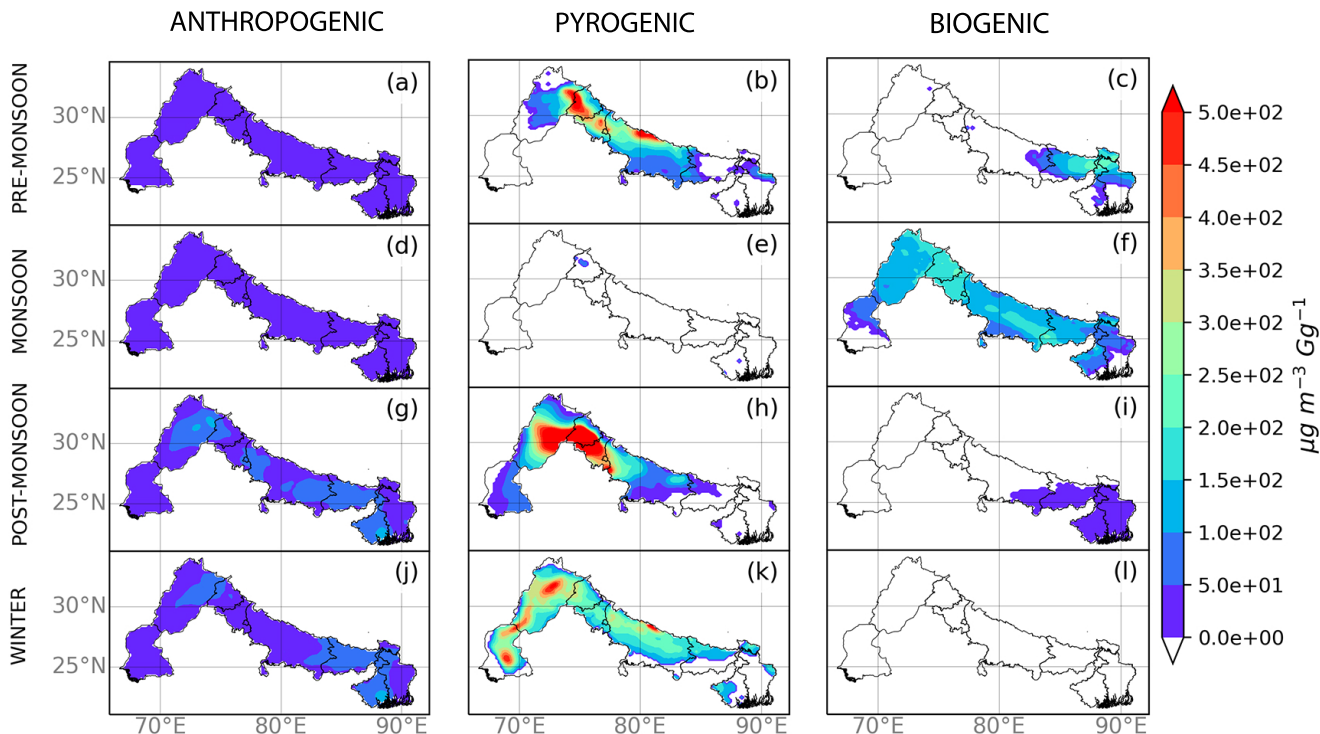
Figure 7. Seasonal sensitivity of total OA to changes in (left column) anthropogenic, (middle column) pyrogenic, and (right column) biogenic emissions (μ g m^{-3}Gg^{-1}). The sensitivity calculation is described in the main text. Regions marked as white shows where sensitivity corresponds to OA concentrations below the set threshold of 1 μg m^{-3}.

Figure 6 shows the season mean distributions of total OA with the corresponding POA and SOA distributions shown by Figures A2 and A3. We generally find that POA dominates seasonal values of total OA across the IGP, with the exception of the post-monsoon season when SOA and POA have comparable values.

During the post-monsoon season (Figure 6g-i), the largest OA concentrations are over the upper IGP at the border of Pakistani and Indian Punjab (> 80 μg m^{-3}), where POA values can exceed 50 μg m^{-3}. Although the largest regional mean is found over the lower IGP (52 μg m^{-3}) due to urban anthropogenic emissions in and around Kolkata and Patna where values are >70 μg m^{-3}. Over the middle IGP, the mean OA value is similar to the lower IGP (52 μg m^{-3}) but shows a more homogeneous distribution, with the highest OA values found at the borders between upper and lower IGP. Regional mean POA values range 23–29 μg m^{-3} (Figure A2g-i), similar to SOA values (20–24 μg m^{-3}, Figure A3g-i). POA levels are much higher than SOA over the Punjab states in India and Pakistan and in the Indian lower IGP (40–70 and 30–40 μg m^{-3} for POA and SOA, respectively). Over the middle IGP, SOA is generally higher than POA (29 and 24 μg m^{-3} for SOA and POA, respectively), with highest concentrations of SOA found in the lower Uttar Pradesh (up to 40 μg m^{-3}). Over Bangladesh and the Pakistani state of Sindth POA and SOA have comparable values (<35 μg m^{-3}).

Similarly to PM$_{2.5}$, we find that during the post-monsoon season, the OA distribution across the IGP is most sensitive to changes in biomass burning emissions (Figure 7g-i), with higher values over the Punjab to Delhi NCT, and part of Uttar Pradesh (up to 10^3 μg m^{-3} where fires are located over Indian Punjab). The sensitivity of OA to changes in biomass burning are localised, with POA most influenced by fires over Punjab and Haryana (Figure A4h) and corresponding impact on SOA extending over Pakistani Punjab and towards the middle IGP (Figure A5h). Similarly, biogenic emissions play only a localised role in OA and SOA concentrations where biogenic emissions are still significant during this season (Figures 7i) and A5i). OA are most sensitive to anthropogenic emissions over the Indian part of the lower IGP and in the **Pakistani Punjab** values (between 50-150 μg m^{-3}). We find that OA over the Delhi NCT megacity is not sensitive to these changes unlike other cities mentioned previously, so that Delhi is not one of the main hotspots of OA across IGP during this season (Figure 6h) unlike it is for PM$_{2.5}$ (Figure 3h). We find that the sensitivity of POA and SOA to changes in anthropogenic emissions are comparable across major cities of the Punjab states (Figures A4g, A5g).

We find that the largest seasonal mean values of OA are during winter over the lower IGP (60 μg m^{-3}, Figure 6j-l) with contributing localised peaks over Kolkata and Patna (>80 μg m^{-3}) and at the border between Pakistan and India (ranging 40–70 μg m^{-3}). Seasonal mean values of POA and SOA also peak during winter over the lower IGP (34 μg m^{-3} and 26 μg m^{-3}, respectively.) During winter, the OA distribution is shaped by anthopogenic and pyrogenic emissions (Figure 7j-l). POA concentrations show to be sensitive to anthropogenic emissions in a similar way as it is for post-monsoon season (Figure A4g,j). SOA is also mostly determined by anthropogenic emissions over the lower IGP (Figure A5j). POA and SOA are also sensitive to pyrogenic emissions, but during this season it is limited to fires over the Indus basin in Pakistan and central IGP (Figures A4k, A5k). We find that biogenic emissions do not significantly influence OA during winter.

During pre-monsoon and monsoon seasons, the OA distributions (Figure 6a-f) have similar mean values over the middle and lower IGP (20–21 μg m^{-3}) and lower mean values over the upper IGP (11 and 18 μg m^{-3}, respectively). The highest POA concentrations are found at the border on India and Pakistan and over the lower IGP ($\simeq$30 and 40 μg m^{-3}, respectively). In both seasons, mean SOA concentrations are below 15 μg m^{-3}) across all the IGP. During pre-monsoon and monsoon seasons, OA concentrations are sensitive to anthropogenic emissions across the IGP with similar spatial distributions (Figure 7a,d). Pyrogenic emissions influence the OA distribution during the pre-monsoon season over the central IGP (Figure 7b), but OA less sensitive to these emissions compared with the post-monsoon season (Figure 7h). During the monsoon season, the influence of fires on OA is negligible across the IGP. The influence of biogenic emissions on OA, determined exclusively in our model via SOA, is limited to the lower IGP during the pre-monsoon season. During the monsoon season, these emissions have a widespread impact on OA (Figure 7f) with seasonal mean peak sensitivity of up to 2.3×10^2 μg m^{-3} Gg^{-1}.

$PM_{2.5}$ **and OA are more sensitive to changes in biogenic emissions than changes in anthropogenic emissions during the monsoon period because of the role that anthropogenic emissions play in controlling the production of biogenic SOA. Previous studies have shown that anthropogenic emissions can enhance biogenic SOA production, with NO$_x$ concentrations playing a strong role in enhancing SOA formation from isoprene, and terpenes (Spracklen et al., 2011; Shilling et al., 2013; Shrivastava et al., 2019; Xu et al., 2020). A disadvantage of our using a single-variable perturbative**
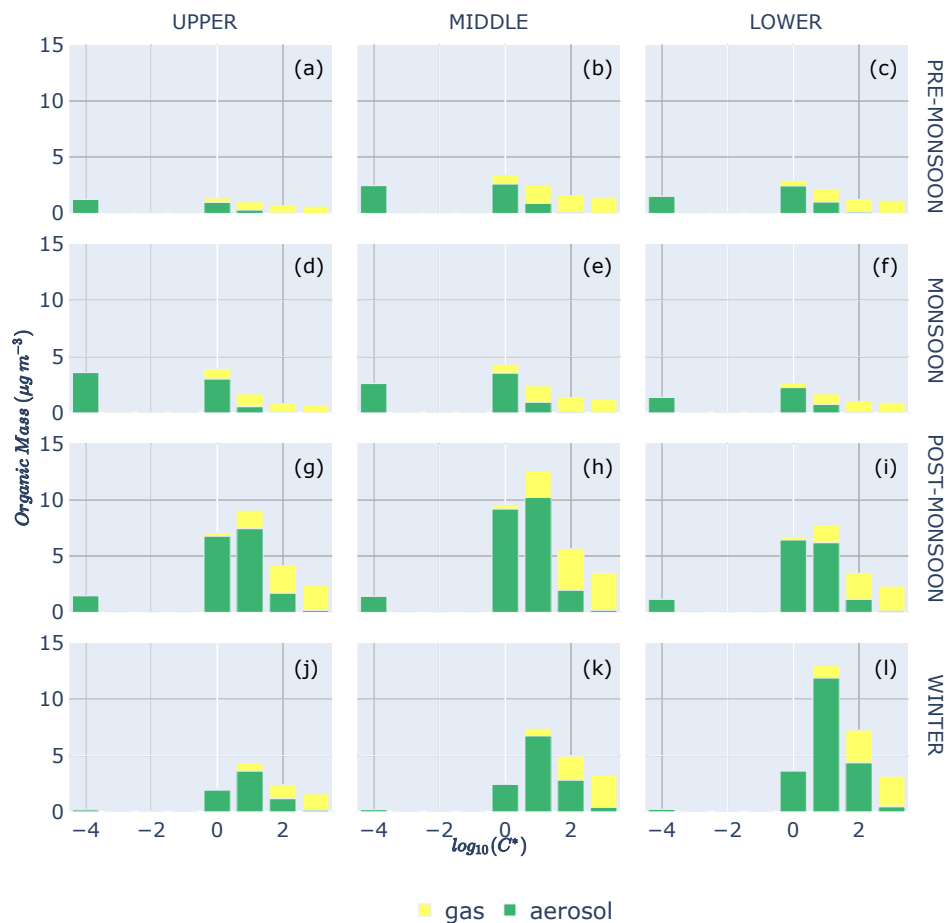
Figure 8. Seasonal mean volatility distribution of SOA over the upper, middle, and lower IGP as calculated within the WRF-Chem 1-D VBS scheme for (a–c) pre-monsoon, (d–f) monsoon, (g–i) post-monsoon, and (j–l) winter seasons.

method is that we can only consider the impacts of one controlling factor in the production of OA. A study that considers the interactions between controlling factors is outside the scope of this study.

3.4 Seasonal Distribution of SOA Volatility

We use aerosol volatility to describe how SOA is partitioned between the gas and particle phase to understand when it con-
470 tributes to PM$_{2.5}$ mass loading. Figure 8 shows the seasonal mean volatility distributions for SOA across the IGP simulated using the 1-D VBS model in WRF-Chem (Knote et al., 2015). Seasonal and regional variations reflect changes in the physical and chemical environment in which the SOA is formed. Broadly, we find a gradual increase in the volatility of SOA from the

pre-monsoon season to the winter season, mainly reflecting the increase in the mean OA loading (Figure 6). Higher OA loading leads to a shift in the gas-particle partitioning towards more volatile bins, reflected in the seasonal variation in the population of the inert bin (denoted here as $log_{10}C^* = -4$, as described above). The contribution of this inert bin is negligible during winter and peaks during the monsoon season, with intermediate values during the pre-monsoon and post-monsoon transition seasons.

During the post-monsoon season, the particle phase organic mass is present at high volatility bins up to $log_{10}C^* = 2$. The largest particle phase mass loading (10 μg m^{-3}) is found over the middle IGP. The upper and lower IGP show a similar volatility distribution as the middle IGP but with lower mass loadings, with the lower IGP having the lowest mass loadings. The smallest values over the lower IGP reflect the persistence of rainfall over this region that leads to continued removal of water soluble gas-phase and aerosol-phase organics.

Surface-level atmospheric organic mass becomes even more volatile during the winter season, with particle phase organic matter present in all volatility bins. The largest mass loading for SOA are found over the lower IGP (> 10 μg m^{-3}) and decreases westwards towards the upper IGP, reflecting the E-W gradient of the total OA loading (Figure 6j–l).

SOA during the pre-monsoon (Figure 8 a–c) and monsoon (Figure 8 d–f) seasons are characterised by a volatility $\leq log_{10}C^* = 1$, and with aerosol masses lower than 5 μg m^{-3} for each volatility bin in both seasons. The higher volatility bins ($log_{10}C^* = 2$ and $\mathbf{log_{10}C^* = 3}$) are occupied exclusively by gas-phase organic compounds. We attribute this to water-soluble SVOCs being washed out by monsoonal rainfall. The washout of SVOCs results in gas-aerosol re-partitioning to establish thermodynamic equilibrium, associated with particle phase organics partitioning to the gas-phase. Aerosols are also removed via wet and dry deposition but we find most of the loss of SVOCs and SOA mass is lost via the gas phase (Knote et al., 2015). This also helps to explain the low levels of OA during the pre-monsoon and monsoon seasons (Figure 6). The OA volatility distribution is similar across the IGP, reflecting an approximately uniform physical environment during the two seasons (Figures A1 and 7).

4   Concluding Remarks

We used the WRF-Chem regional atmospheric chemistry model to understand the influence of anthropogenic, pyrogenic and biogenic emissions and meteorology on seasonal variations of the magnitude, distribution, and composition of PM$_{2.5}$ and organic aerosol across the Indo-Gangetic Plain (IGP) during 2017/2018.

We find that the model reasonably reproduces concentrations of PM$_{2.5}$ in all seasons (NMB<0.2, r>0.6) except for the monsoon season (NMB=0.4, r=0.09), a reflection that modelling monsoonal meteorology remains challenging. However, uncertainty in our estimates remains on the individual PM$_{2.5}$ secondary components, given the limitation we found in the modeling to reproduce precursors gases surface concentrations when compared with observations. Availability of additional monitoring stations outside urban areas that are more representative of the spatial scales associated with model grid cells would help to evaluate model error, as well as use of finer-resolution and up to date inventories for precursors gases over the rapidly changing region of IGP.

We find that the IGP experiences the highest seasonal mean levels of $PM_{2.5}$ during the post-monsoon (October—December, 166 $\mu g\ m^{-3}$) and winter (January—February, 145 $\mu g\ m^{-3}$) seasons with an heterogeneous distribution, in agreement with previous studies. The magnitude and distribution of anthropogenic emissions across the IGP are approximately constant throughout the year. During the post-monsoon season, agricultural burning emissions of post-harvest residues influence $PM_{2.5}$ mostly over the upper and middle IGP, particularly affecting the Indian and Pakistani Punjab region. These additional emissions are exacerbated by high pressure weather systems that reduce ventilation of surface air pollution to the free troposphere. During the winter season, ongoing anthropogenic emissions, wind patterns, and a seasonally shallow boundary layer result in a gradient in air quality from the upper to lower IGP, with the highest $PM_{2.5}$ values (in excess of 250 $\mu g\ m^{-3}$) over Kolkata and the state of Bihar. During the pre-monsoon (March–May) and monsoon (June–September) seasons wet scavenging of hydrophilic gas-phase aerosol precursors and aerosols, and more rigorous vertical mixing, reduces levels of $PM_{2.5}$ (95-79 $\mu g\ m^{-3}$ respectively).Generally, we find that $PM_{2.5}$ composition has a stronger seasonal variation than a geographical variation within each season. Total inorganic species dominate $PM_{2.5}$ composition (30-80%), with water uptake contributing substantially to the $PM_{2.5}$ mass especially over the lower IGP (up to 40%).

We find that OA represents a significant contribution to $PM_{2.5}$ throughout the year. On an annual mean basis, OA represents 17–30% of $PM_{2.5}$, with higher contributions during post-monsoon and winter seasons. Typically, POA contributes more to the OA loading than SOA in all seasons across the IGP. Anthropogenic and pyrogenic sources impact POA and SOA with similar patterns of $PM_{2.5}$ across the IGP during all seasons. Biogenic sources have a significant impact on SOA distribution across the IGP during the monsoon season but are limited to the lower IGP during the pre- and post- monsoon seasons. We find that the volatility distribution of SOA is driven mainly by the mean total OA loading and the washout of aerosols and gas-phase aerosol precursors that result in SOA being less volatile during the pre-monsoon and monsoon season than during the post-monsoon and winter seasons.

Mitigating levels of $PM_{2.5}$ over the IGP will require a range of regional and state-level policies that address the influences of intra- and inter- state anthropogenic, pyrogenic, and biogenic emissions. The relative influence of these emissions on $PM_{2.5}$ and the broader photochemical environment will likely change in the context of a warmer climate, e.g. biogenic emissions will increase as they are temperature dependent. It is therefore imperative that future studies should also consider sub-regional and city spatial scales, where individual sectors will be more important, and where there is the highest population density that will suffer from poor air quality.

Appendix A: Meteorological drivers, POA and SOA distribution

Figure A1 shows the mean seasonal WRF-Chem meteorological driver or pre-monsoon, monsoon and post-monsoon 2017 and winter 2018. Figure A2, to A5 show POA and SOA distribution over the IGP and their sensitivity to emissions drivers.
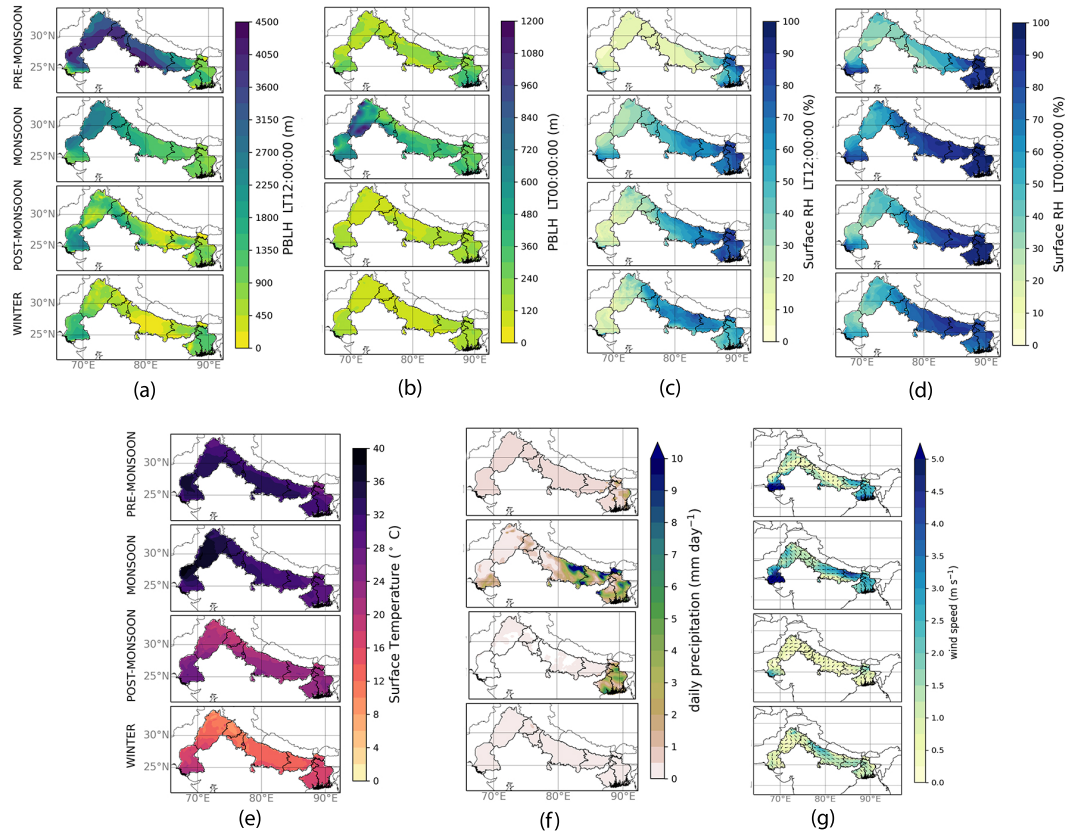
Figure A1. Seasonal mean WRF-Chem meteorological fields: (a) daytime planetary boundary layer height (m); (b) nighttime planetary boundary layer height (m); (c) daytime surface relative humidity (%); (d) nighttime surface relative humidity (%); (e) surface temperature at 2 m (°C; (f) daily precipitation rate (mm day^{-1})); and (g) wind speed (m s^{-1}) and direction at 10 m.
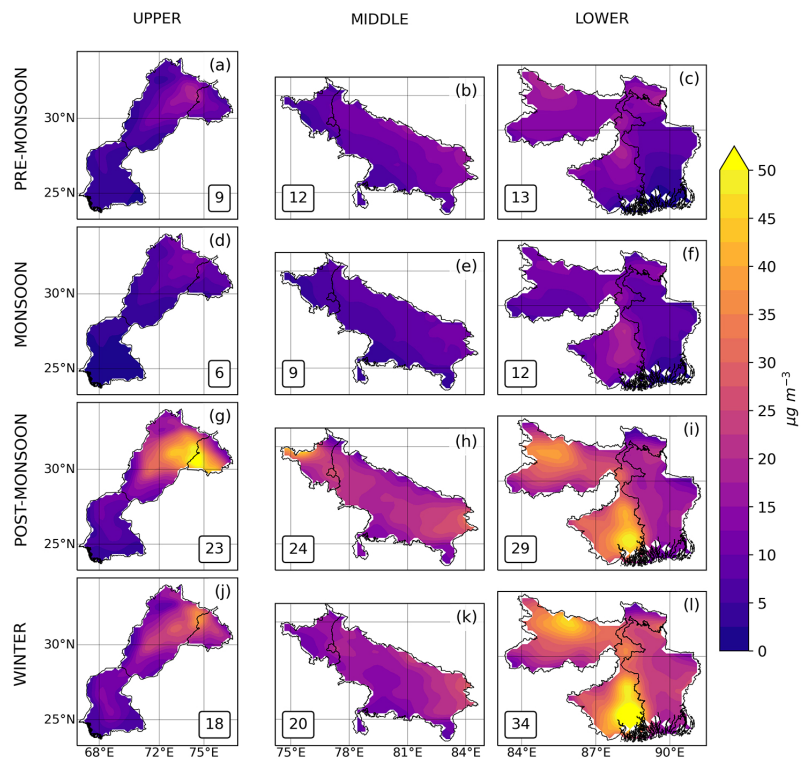
Figure A2. Seasonal mean distributions of POA over the upper, middle and lower IGP. The numbers inset of pre-monsoon (a–c), monsoon (d–f), post-monsoon g–i), and winter (j–l) seasons denote the regional mean POA value.
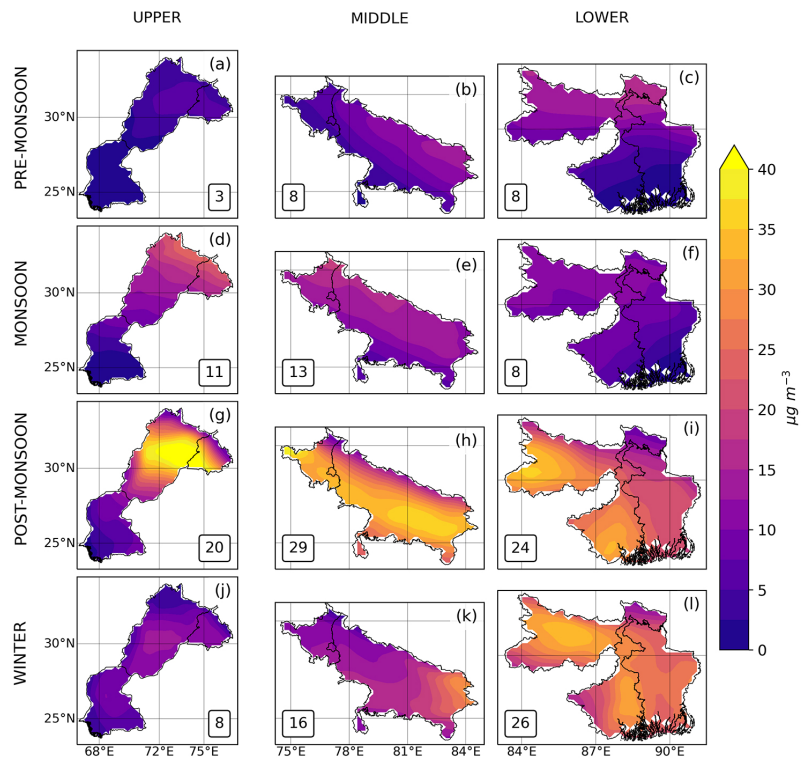
Figure A3. As A2 but for SOA.
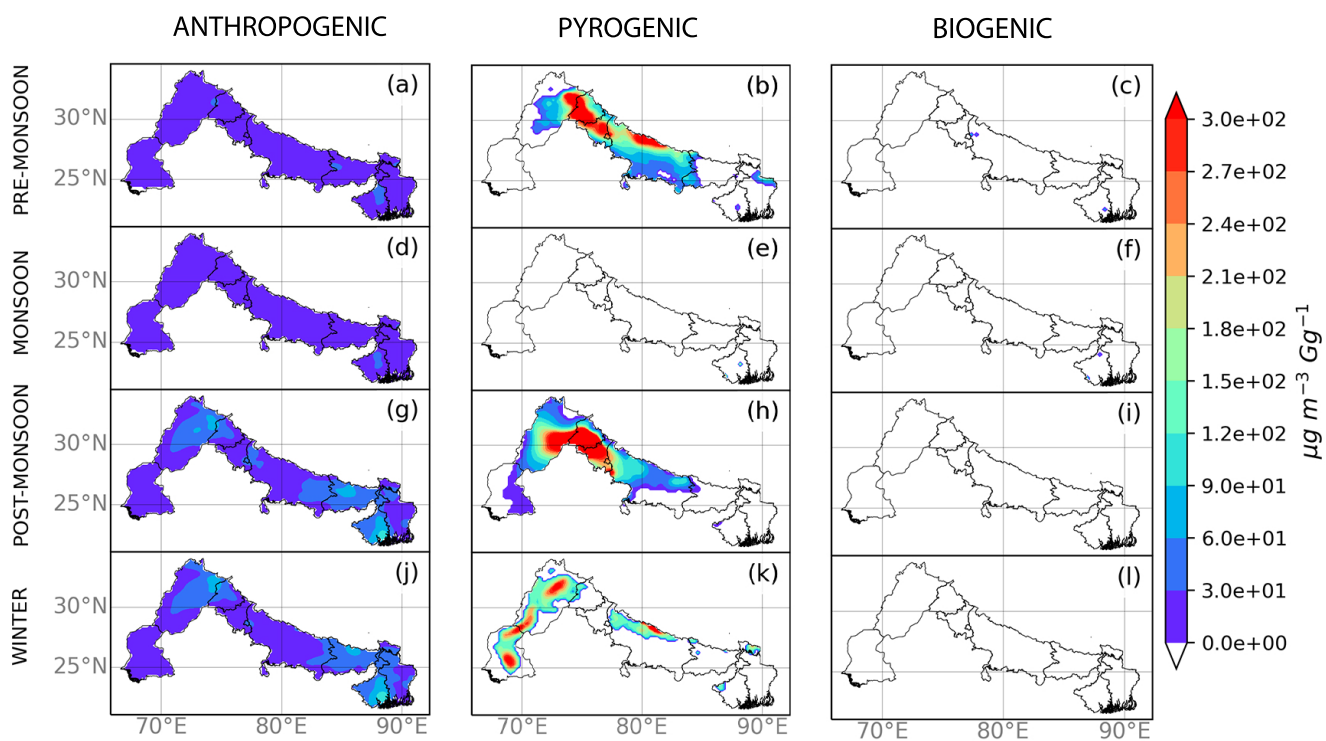
Figure A4. Seasonal sensitivity of POA to changes in (left column) anthropogenic, (middle column) pyrogenic, and (right column) biogenic emissions (μ g m^{-3}Gg^{-1}). The sensitivity calculation is described in the main text. Regions marked as white shows where sensitivity corresponds to OA concentrations below the set threshold of 1 μg m^{-3}.
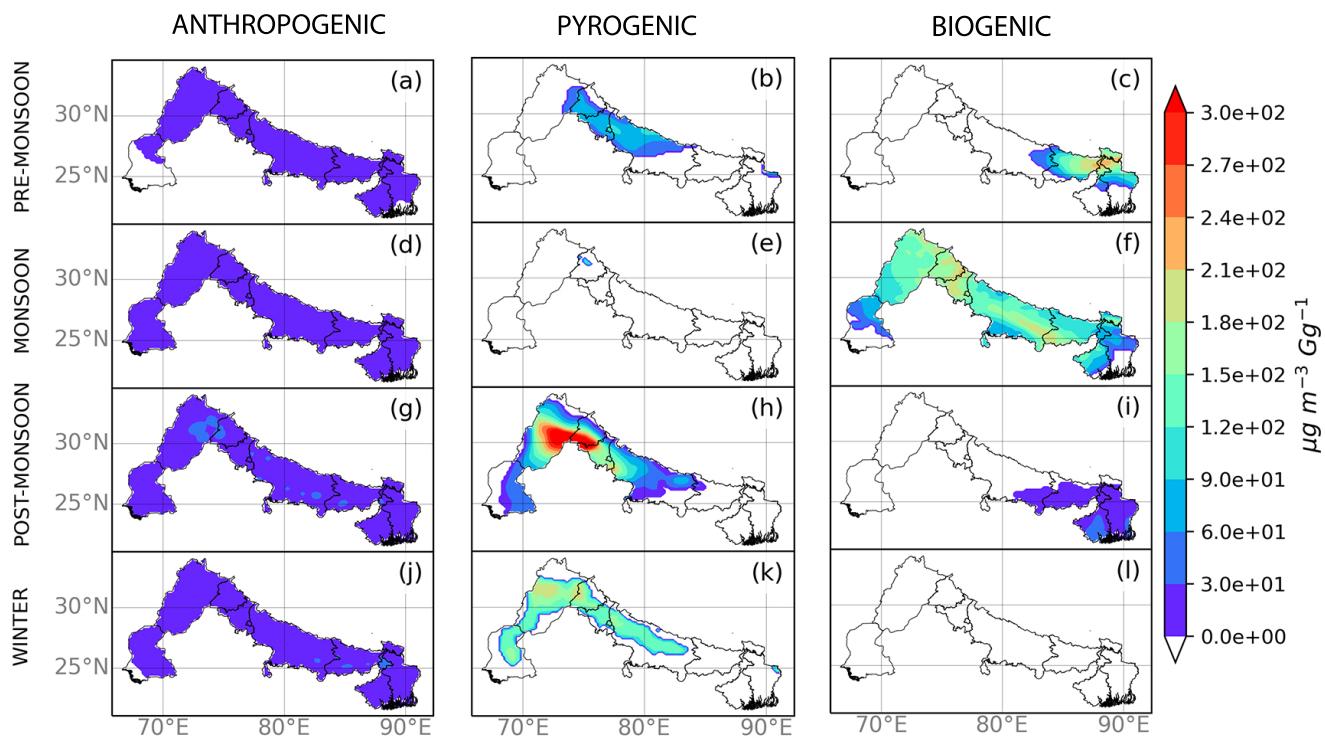
Figure A5. As Figure A4 but for SOA.

Appendix B: WRF-Chem set-up and evaluation

Table B1 summarises the parametrisation for meteorology we use in WRF-Chem. The following subsections describe the evaluation of model result with ground based observation, OA values from literature and with satellite AOD respectively.

B1   Ground-based Measurements evaluation

We use ground-based measurements from the Central Pollution Control Board and the U.S. Embassies, which are available for our 2017/2018 study period, and accessed through the OpenAQ Platform (OpenAQ). Data from Pakistan are only available from 2019 so we use 2019 data for the monsoon and post-monsoon seasons and data from 2020 for the winter and pre-monsoon seasons.

We apply a cleaning procedure of data for each pollutant. The cleaning procedure followed five sequential steps: 1) Exclude non valid, negative and zero values; 2) exclude hourly data with $z_{score} \geq 3$ respect to daily mean; 3) exclude days with fewer **than** 12 hourly measurements per day; 4) exclude stations with less then 15 days measurements per simulated season; and 5) exclude all stations but one if there are multiple stations in the same model grid-cell (for statistical independence in the comparison). From this cleaning procedure we get 31 independent stations (Table B2, **Figure B1**) with a total of seasonal measurements: 63 for CO, 54 for SO_2, 61 for NO_2, 50 for O_3, 84 for $PM_{2.5}$, 20 for PM_{10}. For particulate matter, we compare the dry mass of $PM_{2.5}$ and PM_{10}.

To compare the model against these measurements, we sample the model at the time and location of each measurement. In practice, we identify the model value closest to the measurement. We report seasonal mean statistics.

We evaluate the model using five metrics: the Mean Bias (MB), Root Mean Square Error (RMSE), Normalised Mean Bias (NMB), Mean Normalised Absolute Error (MNAE), and sample Pearson correlation coefficient (r). These metrics are widely used for air quality model evaluation (Zhang et al., 2006; Kumar et al., 2012b; Brasseur and Jacob, 2017; Conibear et al., 2018). Table B3 summarises the seasonal mean evaluation of the model with the metrics described.

B2   Organic Aerosols

In the absence of continuous monitoring data of OA, we compare our model OC values with values found in the literature. Table B4 shows the comparison of modeled OC with measurements studies. **Location of measurement sites is shown in Figure B1** OA are converted from organic aerosol mass to organic carbon mass assuming OA/OC ratios 1.4 for POA and 2.0 for SOA, following (Knote et al., 2015).

B3   Total AOD column

We compare our modeled prediction against satellite AOD retrievals **for 2017/2018** at 550 nm with a 10 km horizontal resolution obtained from both Terra (MOD04_L2) and Aqua (MYD04_L2) MODIS instruments. We use the best-quality AOD retrievals merged from the dark target and the deep blue algorithms (Levy et al., 2013). We re-grid the 10 km Terra and Aqua MODIS AOD data to the coarse WRF-Chem 20 km×20 km model grid.

We calculate the 550 nm AOD using WRF-Chem values at 300 nm and 1000 nm by interpolation using the Ångström power law. We sample the model at the local overpass time of Terra (1030) and Aqua (1330) where there exists at least one best-quality AOD retrieval. We then mean model and MODIS AOD values over time to generate seasonal statistics. Table B5 reports the main statistical metrics for AOD evaluation together with the range of observed and modeled AOD.
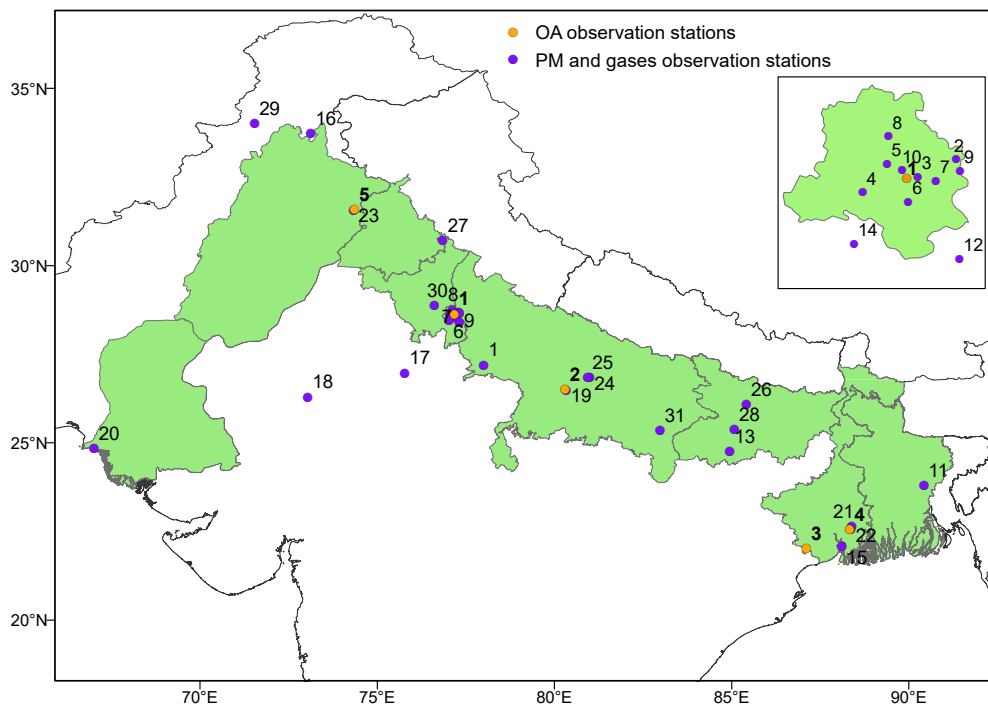
Figure B1. Location of ground based observation for PM and gases (purple) and OA (orange). ID Number for each station correspond to ID number in table A2 and A4 respectively. The inset map shows in detail Delhi NCT.

Table B1. Chosen parametrisations for meteorological processes in WRF-Chem.

Process	Parametrisation
Cloud microphysics	Morrison double-moment scheme (Morrison et al., 2005)
Planetary boundary layer	Mellor-Yamada Nakanishi and Niino 2.5 (MYNN2) (Nakanishi and Niino, 2006)
Convection	Grell 3D scheme (Grell and Dévényi, 2002).
Short and long wave radiation	The Rapid Radiative Transfer Model (RRTM) (Iacono et al., 2008).
Land surface	Noah Land Surface Model coupled with a urban canopy model (Ek et al., 2003; Kusaka and Kimura, 2004)

Table B2. List of selected ground-based stations and their measurements used for model evaluation.

number ID	city	station name	latitude	longitude
1	Agra	Sanjay Palace	27.20	78.01
2	Delhi	Income Tax Office	28.62	77.25
3	Delhi	Delhi Technological University	28.74	77.12
4	Delhi	Shadipur	28.65	77.16
5	Delhi	Anand Vihar	28.65	77.32
6	Delhi	Punjabi Bagh	28.67	77.12
7	Delhi	NSIT Dwarka	28.59	77.05
8	Delhi	IHBAS	28.68	77.31
9	Delhi	Mandir Marg	28.63	77.20
10	Delhi	R K Puram	28.56	77.17
11	Dhaka	US Diplomatic Post: Dhaka	23.80	90.42
12	Faridabad	Sector16A Faridabad	28.41	77.31
13	Gaya	Collectorate - Gaya - BSPCB	24.75	84.94
14	Gurgaon	Vikas Sadan Gurgaon - HSPCB	28.45	77.03
15	Haldia	Haldia - WBPCB	22.06	88.11
16	Islamabad	US Diplomatic Post: Islamabad	33.72	73.12
17	Jaipur	VK Industrial Area Jaipur - RSPCB	26.97	75.77
18	Jodhpur	Collectorate Jodhpur - RSPCB	26.29	73.04
19	Kanpur	Nehru Nagar	26.47	80.33
20	Karachi	US Diplomatic Post: Karachi	24.84	67.01
21	Kolkata	US Diplomatic Post: Kolkata	22.56	88.36
22	Kolkata	Rabindra Bharati University, Kolkata - WBSPCB	22.63	88.38
23	Lahore	US Diplomatic Post:Lahore	31.56	74.34
24	Lucknow	Central School	26.85	81.00
25	Lucknow	Lalbagh, DN Park	26.85	80.94
26	Muzaffarpur	Collectorate - Muzaffarpur - BSPCB	26.08	85.41
27	Panchkula	Sector 6 Panchkula - HSPCB	30.71	76.85
28	Patna	IGSC Planetarium Complex - Patna - BSPCB	25.36	85.08
29	Peshawar	US Diplomatic Post: Peshawar	34.01	71.54
30	Rohtak	MD University, Rohtak - HSPCB	28.88	76.62
31	Varanasi	Ardhali Bazar	25.35	82.98

Table B3. Statistical evaluation of model performance with ground based measurements for main PM and main gas pollutants.

pollutant	season	NMB	NMAE	MB [$\mu g\ m^{-3}$]	RMSE [$\mu g\ m^{-3}$]	r
$PM_{2.5}$	pre-monsoon	0.12	0.31	10	34	0.62
	monsoon	0.41	0.65	19	36	0.09
	post-monsoon	0.19	0.28	33	62	0.84
	winter	0.004	0.28	0.7	53	0.69
PM_{10}	pre-monsoon	0.15	0.59	32	133	0.11
	monsoon	-0.21	0.28	-25	46	0.69
	post-monsoon	-0.14	0.36	-41	122	0.66
	winter	-0.25	0.43	-64	131	-0.85
CO	pre-monsoon.	-0.64	0.64	-643	825	0.44
	monsoon	-0.55	0.55	-428	567	0.12
	post-monsoon	-0.65	0.65	-1439	2272	0.29
	winter	-0.52	0.61	-703	1163	-0.20
NO_2	pre-monsoon	0.14	0.95	6	57	0.27
	monsoon	0.46	1.00	11	32	0.08
	post-monsoon	0.65	1.44	36	97	0.15
	winter	0.31	0.98	17	66	0.30
O_3	pre-monsoon	1.59	1.67	75	91	-0.52
	monsoon	2.92	2.92	64	66	-0.12
	post-monsoon	2.96	2.98	98	113	-0.75
	winter	2.87	2.92	71	87	-0.55
SO_2	pre-monsoon	0.25	0.85	3	13	0.04
	monsoon	0.27	1.38	4	34	-0.18
	post-monsoon	2.36	2.44	33	49	0.51
	winter	1.85	2.15	27	43	0.04

Table B4. Comparison of modeled OC with measurements studies in the literature. Model values refers to the mean over the corresponding season of observations.

number ID	location	period	species	OC obs [$\mu g\ m^{-3}$]	OC model [$\mu g\ m^{-3}$]	reference
1	Delhi	Jan-Feb 13-16	PM$_{2.5}$	23.6 ± 12.9	23.4	Jain et al. (2020)
		Mar-May 13-16		9.82 ± 4.16	13.3	
		Jun-Set 13-16		6.77 ±2.63	12.1	
		Oct-Dec 13-16		25.2 ±14.7	38.6	
1	Delhi	Jan-Feb 13-16	PM$_{10}$	30.1±12.1	23.5	Jain et al. (2020)
		Mar-May 13-16		23.4 ± 10.7	13.4	
		Jun-Set 13-16		15.9 ±9.7	12.3	
		Oct-Dec 13-16		39.4 ±15.6	38.7	
2	Kanpur	Oct-Nov 08	PM$_{10}$	53.3 ±21.2	37.2	Ram et al. (2012)
		Dec 08 - Feb 09		29 ± 14.5	21.9	
		Mar-Apr 09		23.1 ± 11.5	12.3	
3	Kharagpur	Nov 09 - Mar 10	PM$_{2.5}$	30.7± 12.1	42.0	Srinivas and Sarin (2014)
4	Kolkata	Jan-06	PM$_{2.5}$	18.5±2.0	67.2	Chatterjee et al. (2012)
		Apr-May 06		15.5± 3.6	7.8	
		Jul-06		5±1	14.3	
		Oct-Nov 06		11.5±5.0	57.4.	
5	Lahore	Jan-07	PM$_{2.5}$	76.5	34.0	Stone et al. (2010)
		Apr-May-07		43.5	20.0	
		Jul-07		31.5	18.2	
		Oct-Nov 07		111.2	61.0	

Table B5. Seasonal comparison of modeled total AOD column and satellite AOD observations for the Terra and Aqua instruments over the IGP **for the simulated period 2017/2018**.

satellite	season	MB	NMB	NMAE	RMSE	r	range obs	range model
Terra	pre-monsoon	0.33	0.53	0.56	0.44.	0.53	0.06 - 1.78	0.10 - 2.29
	monsoon	0.04	0.05	0.45	0.52	0.35	0.00 - 3.42	0.10 - 3.78
	post-monsoon	-0.05	-0.06	0.25	0.25	0.76	0.07 - 3.50	0.12 - 1.71
	winter	-0.11	-0.19	0.30	0.21	0.64	0.05 - 1.74	0.11 - 1.16
Aqua	pre-monsoon	0.27	0.44	0.49	0.40	0.52	0.07 - 3.50	0.08 - 2.82
	monsoon	-0.18	-0.19	0.43	0.53.	0.35	0.04 - 2.53	0.11 - 3.17
	post-monsoon	-0.05	-0.06	0.25	0.23	0.74	0.06 - 2.23	0.12 - 1.47
	winter	-0.08	-0.14	0.33	0.22	0.47	0.09 - 1.17	0.08 - 1.2

Code and data availability. All the data and materials used in this study are freely available. The WRF-Chem model code is available from https://www2.acom.ucar.edu/wrf-chem. NCEP FNL global tropospheric analyses were taken from https://rda.ucar.edu/datasets/ds083.3/. CAM-CHEM global model results were downloaded from https://www.acom.ucar.edu/cam-chem/cam-chem.shtml. The EDGAR-HTAPv2.2 emissions dataset ready for be used in WRF-Chem were downloaded from https://www2.acom.ucar.edu/wrf-chem/wrf-chem-tools-community. The FINN biomass burning emissions dataset was downloaded from https://bai.acom.ucar.edu/Data/fire/. Ground based observation used for the model evaluation where obtained from https://openaq.org/. The MODIS data are available from https://ladsweb.modaps.eosdis.nasa.gov/. Metadata and code that describe our calculations are temporarily stored at https://github.com/catemgn/aqIGP; we will move metadata and code to a permanent repository once the paper has been accepted for publication.

Author contributions. CM and PIP conceived the study and methodology. CM set-up the model with support from CK. CM performed the simulations, and led the model evaluation and data analysis, and interpreted the results together with PIP, CK and TJW. FY provided the AOD observations to be compared with the model AOD. CM and PIP wrote the paper, with input from all co-authors.

Competing interests. The authors declare that they have no conflict of interest.

Acknowledgements. CM is supported by funding from the Ford Motor Company University Research Program (#2016-2007R). The work of Fei Yao was supported by the China Scholarships Council/University of Edinburgh Scholarships. This study was funded as part of NERC's support of the National Centre for Earth Observation: PIP was supported by grant number #NE/R016518/1. We thank Jim Anderson, Wei Shen, and Sandy Winkler for helpful discussions. CM is thankful to the WRF-Chem community for the support received, in particular to S. Walters, G. Pfister, M. Barth, for providing support in the WRF-Chem online forum, and to L. Conibear, D. Lowe, R. Kumar, S. Archer-Nicholls, M. Morichetti for discussion and clarifications on specific technical issues. We acknowledge the use of the WRF-Chem preprocessor tool (anthro-emiss, fire-emiss, bioemiss, mozbc) provided by the Atmospheric Chemistry Observations and Modeling Lab (ACOM) of NCAR. We also acknowledge the use of the following software and packages for the post-processing and analysis of WRF-Chem simulations: ArcGIS 10.7, Python 3.6, xarray (Hoyer and Hamman, 2017), pandas (The pandas dev. Team, 2020) numPy (Harris et al., 2020) cartopy (Met Office, 2010 - 2015), plotly (Plotly Technologies Inc., 2015), matplotlib (Hunter, 2007), salem (Maussion et al., 2017). Administrative areas for IGP were taken from GADM (https://gadm.org).

References

ACOM-NCAR: WRF-Chem Tools for the Community, https://www2.acom.ucar.edu/wrf-chem/wrf-chem-tools-community, last access: 30 November 2020.

Agarwala, M. and Chandel, A.: Temporal role of crop residue burning (CRB) in Delhi's air pollution, Environ. Res. Lett., 15, 114 020, https://doi.org/https://doi.org/10.1088/1748-9326/abb854, 2020.

Ahmadov, R., McKeen, S., Robinson, A., Bahreini, R., Middlebrook, A., De Gouw, J., Meagher, J., Hsie, E.-Y., Edgerton, E., Shaw, S., et al.: A volatility basis set model for summertime secondary organic aerosols over the eastern United States in 2006, J. Geophys. Res.-Atmos., 117, https://doi.org/https://doi.org/10.1029/2011JD016831, 2012.

Ahmed, T., Ahmad, B., and Ahmad, W.: Why do farmers burn rice residue? Examining farmers' choices in Punjab, Pakistan, Land Use Policy, 47, 448–458, https://doi.org/https://doi.org/10.1016/j.landusepol.2015.05.004, 2015.

Alam, K., Mukhtar, A., Shahid, I., Blaschke, T., Majid, H., Rahman, S., Khan, R., Rahman, N., et al.: Source apportionment and characterization of particulate matter (PM_{10}) in urban environment of Lahore, Aerosol Air Qual. Res., 14, 1851–1861, https://doi.org/https://doi.org/10.4209/aaqr.2014.01.0005, 2014.

Balasubramanian, S., McFarland, D. M., Koloutsou-Vakakis, S., Fu, K., Menon, R., Lehmann, C., and Rood, M. J.: Effect of grid resolution and spatial representation of NH3 emissions from fertilizer application on predictions of NH3 and PM2.5 concentrations in the United States Corn Belt, Environ. Res. Commun., 2, 025 001, https://doi.org/https://doi.org/10.1088/2515-7620/ab6c01, 2020.

Bangladesh Bureau of Statistics: Population and housing census 2011, Tech. rep., Statistics Division Ministry of Planning Government of the People's Republic of Bangladesh, 2011.

Begum, B. A., Hopke, P. K., and Markwitz, A.: Air pollution by fine particulate matter in Bangladesh, Atmos. Pollut. Res., 4, 75–86, https://doi.org/https://doi.org/10.5094/APR.2013.008, 2013.

Behera, S. N. and Sharma, M.: Spatial and seasonal variations of atmospheric particulate carbon fractions and identification of secondary sources at urban sites in North India, Environ. Sci. Pollut. R., 22, 13 464–13 476, https://doi.org/https://doi.org/10.1007/s11356-015-4603-7, 2015.

Bergström, R., Denier Van Der Gon, H., Prévôt, A. S., Yttri, K. E., and Simpson, D.: Modelling of organic aerosols over Europe (2002–2007) using a volatility basis set (VBS) framework: application of different assumptions regarding the formation of secondary organic aerosol, Atmos. Chem. Phys., 12, 8499–8527, 2012.

Bhowmik, H. S., Naresh, S., Bhattu, D., Rastogi, N., Prévôt, A. S., and Tripathi, S. N.: Temporal and spatial variability of carbonaceous species (EC; OC; WSOC and SOA) in $PM_{2.5}$ aerosol over five sites of Indo-Gangetic Plain, Atmos. Pollut. Res., https://doi.org/https://doi.org/10.1016/j.apr.2020.09.019, 2020.

Bran, S. H. and Srivastava, R.: Investigation of $PM_{2.5}$ mass concentration over India using a regional climate model, Environ. Pollut., 224, 484–493, https://doi.org/https://doi.org/10.1016/j.envpol.2017.02.030, 2017.

Brasseur, G. P. and Jacob, D. J.: Modeling of atmospheric chemistry, Cambridge University Press, 2017.

Buchholz, R. R., Emmons, L. K., and Tilmes, S. a.: CESM2.1/CAM-chem Instantaneous Output for Boundary Conditions, https://doi.org/10.5065/NMP7-EP60, subset: Lat: 0 to 50, Lon: 50 to 100, October 2017 - February 2018, Accessed 29 March 2020, 2019.

Chatterjee, A., Dutta, C., Jana, T., and Sen, S.: Fine mode aerosol chemistry over a tropical urban atmosphere: characterization of ionic and carbonaceous species, J. Atmos. Chem., 69, 83–100, https://doi.org/https://doi.org/10.1007/s10874-012-9231-8, 2012.

630   Chauhan, B. S., Mahajan, G., Sardana, V., Timsina, J., and Jat, M. L.: Productivity and sustainability of the rice–wheat cropping system in the Indo-Gangetic Plains of the Indian subcontinent: problems, opportunities, and strategies, in: Adv. Agron., vol. 117, pp. 315–369, Elsevier, https://doi.org/https://doi.org/10.1016/B978-0-12-394278-4.00006-4, 2012.

     Chowdhury, Z., Zheng, M., Schauer, J. J., Sheesley, R. J., Salmon, L. G., Cass, G. R., and Russell, A. G.: Speciation of ambient fine organic carbon particles and source apportionment of $PM_{2.5}$ in Indian cities, J. Geophys. Res.-Atmos., 112,
635   https://doi.org/https://doi.org/10.1029/2007JD008386, 2007.

     Chuang, W. K. and Donahue, N. M.: A two-dimensional volatility basis set–Part 3: Prognostic modeling and NOx dependence, Atmos. Chem. Phys., 16, 123–134, https://doi.org/https://doi.org/10.5194/acp-16-123-2016, 2016.

     Conibear, L., Butt, E. W., Knote, C., Arnold, S. R., and Spracklen, D. V.: Residential energy use emissions dominate health impacts from exposure to ambient particulate matter in India, Nat. Commun., 9, 1–9, https://doi.org/https://doi.org/10.1038/s41467-018-02986-7, 2018.

640   Conibear, L. A., Butt, E. W., Knote, C., Lam, N. L., Arnold, S., Tibrewal, K., Venkataraman, C., Spracklen, D. V., and Bond, T. C.: A complete transition to clean household energy can save one–quarter of the healthy life lost to particulate matter pollution exposure in India, Environ. Res. Lett., https://doi.org/https://doi.org/10.1088/1748-9326/ab8e8a, 2020.

     CPCB: Air Quality Automatic Monitoring Data, https://app.cpcbccr.com/ccr/#/caaqm-dashboard-all/caaqm-landing, last access: 30 November 2020.

645   David, L. M., Ravishankara, A., Kodros, J. K., Pierce, J. R., Venkataraman, C., and Sadavarte, P.: Premature mortality due to $PM_{2.5}$ over India: Effect of atmospheric transport and anthropogenic emissions, GeoHealth, 3, 2–10, https://doi.org/https://doi.org/10.1029/2018GH000169, 2019.

     DESA, U.: 2018 Revision of World Urbanization Prospects, Tech. rep., United Nation Department of Economic and Social Affairs, 2018.

     Donahue, N., Robinson, A., Stanier, C., and Pandis, S.: Coupled partitioning, dilution, and chemical aging of semivolatile organics, Environ.
650   Sci. Technol., 40, 2635–2643, https://doi.org/https://doi.org/10.1021/es052297c, 2006.

     Donahue, N. M., Kroll, J., Pandis, S. N., and Robinson, A. L.: A two-dimensional volatility basis set–Part 2: Diagnostics of organic-aerosol evolution, Atmos. Chem. Phys., 12, 615–634, https://doi.org/https://doi.org/10.5194/acp-12-615-2012, 2012.

     Ek, M., Mitchell, K., Lin, Y., Rogers, E., Grunmann, P., Koren, V., Gayno, G., and Tarpley, J.: Implementation of Noah land surface model advances in the National Centers for Environmental Prediction operational mesoscale Eta model, J. Geophys. Res.-Atmos., 108,
655   https://doi.org/https://doi.org/10.1029/2002JD003296, 2003.

     Emmons, L. K., Walters, S., Hess, P. G., Lamarque, J.-F., Pfister, G. G., Fillmore, D., Granier, C., Guenther, A., Kinnison, D., Laepple, T., et al.: Description and evaluation of the Model for Ozone and Related chemical Tracers, version 4 (MOZART-4), Geosci. Model Dev., 3, 43–67, https://doi.org/https://doi.org/10.5194/gmd-3-43-2010, 2010.

     Fountoukis, C., Koraj, D., Van Der Gon, H. D., Charalampidis, P., Pilinis, C., and Pandis, S.: Impact of grid resolution on the predicted fine PM
660   by a regional 3-D chemical transport model, Atmos. Environ., 68, 24–32, https://doi.org/https://doi.org/10.1016/j.atmosenv.2012.11.008, 2013.

     Friedl, M. A., Sulla-Menashe, D., Tan, B., Schneider, A., Ramankutty, N., Sibley, A., and Huang, X.: MODIS Collection 5 global land cover: Algorithm refinements and characterization of new datasets, Remote Sens. Environ., 114, 168–182, https://doi.org/https://doi.org/10.1016/j.rse.2009.08.016, 2010.

665   Gani, S., Bhandari, S., Seraj, S., Wang, D. S., Patel, K., Soni, P., Arub, Z., Habib, G., Hildebrandt Ruiz, L., and Apte, J. S.: Submicron aerosol composition in the world's most polluted megacity: the Delhi Aerosol Supersite study., Atmos. Chem. Phys., 19, https://doi.org/https://doi.org/10.5194/acp-19-6843-2019, 2019.

Gelaro, R., McCarty, W., Suárez, M. J., Todling, R., Molod, A., Takacs, L., Randles, C. A., Darmenov, A., Bosilovich, M. G., Reichle, R., et al.: The modern-era retrospective analysis for research and applications, version 2 (MERRA-2), J. Climate, 30, 5419–5454, https://doi.org/https://doi.org/10.1175/JCLI-D-16-0758.1, 2017.

Ghude, S. D., Pfister, G. G., Jena, C., Van Der A, R., Emmons, L. K., and Kumar, R.: Satellite constraints of nitrogen oxide (NOx) emissions from India based on OMI observations and WRF-Chem simulations, Geophys. Res. Lett., 40, 423–428, https://doi.org/https://doi.org/10.1002/grl.50065, 2013.

Ghude, S. D., Chate, D., Jena, C., Beig, G., Kumar, R., Barth, M., Pfister, G., Fadnavis, S., and Pithani, P.: Premature mortality in India due to PM$_{2.5}$ and ozone exposure, Geophys. Res. Lett., 43, 4650–4658, https://doi.org/https://doi.org/10.1002/2016GL068949, 2016.

Greenstone, M., , and Fan, C.: Air Quality Life Index, Annual Update, Tech. rep., Energy Policy Institute at The University of Chicago (EPIC), 2020.

Grell, G. A. and Dévényi, D.: A generalized approach to parameterizing convection combining ensemble and data assimilation techniques, Geophys. Res. Lett., 29, 38–1, https://doi.org/https://doi.org/10.1029/2002GL015311, 2002.

Grell, G. A., Peckham, S. E., Schmitz, R., McKeen, S. A., Frost, G., Skamarock, W. C., and Eder, B.: Fully coupled "online" chemistry within the WRF model, Atmos. Enviro., 39, 6957–6975, https://doi.org/https://doi.org/10.1016/j.atmosenv.2005.04.027, 2005.

Guenther, A., Karl, T., Harley, P., Wiedinmyer, C., Palmer, P., and Geron, C.: Estimates of global terrestrial isoprene emissions using MEGAN (Model of Emissions of Gases and Aerosols from Nature), Atmos. Chem. and Phys., 6, 3181–3210, https://doi.org/https://doi.org/10.5194/acp-6-3181-2006, 2006.

Gumma, M. K., Thenkabail, P. S., Teluguntla, P., and Whitbread, A. M.: Indo-Ganges River Basin Land Use/Land Cover (LULC) and Irrigated Area Mapping, in: Indus River Basin, pp. 203–228, Elsevier, https://doi.org/https://doi.org/10.1016/B978-0-12-812782-7.00010-2, 2019.

Gunthe, S. S., Liu, P., Panda, U., Raj, S. S., Sharma, A., Darbyshire, E., Reyes-Villegas, E., Allan, J., Chen, Y., Wang, X., et al.: Enhanced aerosol particle growth sustained by high continental chlorine emission in India, Nat. Geosci., 14, 77–84, https://doi.org/https://doi.org/10.1038/s41561-020-00677-x, 2021.

Guttikunda, S. K. and Gurjar, B. R.: Role of meteorology in seasonality of air pollution in megacity Delhi, India, Environ. Monit. Assess., 184, 3199–3211, https://doi.org/https://doi.org/10.1007/s10661-011-2182-8, 2012.

Guttikunda, S. K. and Jawahar, P.: Atmospheric emissions and pollution from the coal-fired thermal power plants in India, Atmos. Environ., 92, 449–460, https://doi.org/https://doi.org/10.1016/j.atmosenv.2014.04.057, 2014.

Guttikunda, S. K., Goel, R., and Pant, P.: Nature of air pollution, emission sources, and management in the Indian cities, Atmos. Environ., 95, 501–510, https://doi.org/https://doi.org/10.1016/j.atmosenv.2014.07.006, 2014.

Hardacre, C. J., Palmer, P. I., Baumanns, K., Rounsevell, M., and Murray-Rust, D.: Probabilistic estimation of future emissions of isoprene and surface oxidant chemistry associated with land-use change in response to growing food needs, Atmospheric Chemistry and Physics, 13, 5451–5472, https://doi.org/10.5194/acp-13-5451-2013, https://acp.copernicus.org/articles/13/5451/2013/, 2013.

Harris, C. R., Millman, K. J., van der Walt, S. J., Gommers, R., Virtanen, P., Cournapeau, D., Wieser, E., Taylor, J., Berg, S., Smith, N. J., Kern, R., Picus, M., Hoyer, S., van Kerkwijk, M. H., Brett, M., Haldane, A., del R'ıo, J. F., Wiebe, M., Peterson, P., G'erard-Marchant, P., Sheppard, K., Reddy, T., Weckesser, W., Abbasi, H., Gohlke, C., and Oliphant, T. E.: Array programming with NumPy, Nature, 585, 357–362, https://doi.org/10.1038/s41586-020-2649-2, https://doi.org/10.1038/s41586-020-2649-2, 2020.

Hoyer, S. and Hamman, J.: xarray: N-D labeled arrays and datasets in Python, Journal of Open Research Software, 5, https://doi.org/10.5334/jors.148, http://doi.org/10.5334/jors.148, 2017.

Hunter, J. D.: Matplotlib: A 2D graphics environment, Computing in Science & Engineering, 9, 90–95, https://doi.org/10.1109/MCSE.2007.55, 2007.

Iacono, M. J., Delamere, J. S., Mlawer, E. J., Shephard, M. W., Clough, S. A., and Collins, W. D.: Radiative forcing by long-lived greenhouse gases: Calculations with the AER radiative transfer models, J. Geophys. Res.-Atmos., 113, https://doi.org/https://doi.org/10.1029/2008JD009944, 2008.

India Meteorological Department: Frequently Asked Questions (FAQ), http://www.imdsikkim.gov.in/wxfaq.pdf, last access: 30 November 2020.

Indian National Commission on Population: Population projections for India and States 2011-2036, Tech. rep., Indian Ministry of Health Family welfare, 2020.

Jain, S., Sharma, S., Vijayan, N., and Mandal, T.: Seasonal characteristics of aerosols ($PM_{2.5}$ and PM_{10}) and their source apportionment using PMF: A four year study over Delhi, India, Environ. Pollut., p. 114337, https://doi.org/https://doi.org/10.1016/j.envpol.2020.114337, 2020.

Janssens-Maenhout, G., Crippa, M., Guizzardi, D., Dentener, F., Muntean, M., Pouliot, G., Keating, T., Zhang, Q., Kurokawa, J., Wankmüller, R., et al.: HTAP_v2. 2: a mosaic of regional and global emission grid maps for 2008 and 2010 to study hemispheric transport of air pollution, Atmos. Chem. Phys., 15, 11 411–11 432, https://doi.org/https://doi.org/10.5194/acp-15-11411-2015, 2015.

Jethva, H., Satheesh, S., and Srinivasan, J.: Seasonal variability of aerosols over the Indo-Gangetic basin, J. Geophys. Res.-Atmos., 110, https://doi.org/https://doi.org/10.1029/2005JD005938, 2005.

Jethva, H., Chand, D., Torres, O., Gupta, P., Lyapustin, A., and Patadia, F.: Agricultural burning and air quality over northern India: a synergistic analysis using NASA's A-train satellite data and ground measurements, Aerosol Air Qual. Res., 18, 1756–1773, https://doi.org/https://doi.org/10.4209/aaqr.2017.12.0583, 2018.

Jethva, H., Torres, O., Field, R. D., Lyapustin, A., Gautam, R., and Kayetha, V.: Connecting crop productivity, residue fires, and air quality over northern India, Sci. Rep., 9, 1–11, https://doi.org/https://doi.org/10.1038/s41598-019-52799-x, 2019.

Karambelas, A., Holloway, T., Kiesewetter, G., and Heyes, C.: Constraining the uncertainty in emissions over India with a regional air quality model evaluation, Atmos. Environ., 174, 194–203, https://doi.org/https://doi.org/10.1016/j.atmosenv.2017.11.052, 2018.

Knote, C., Hodzic, A., Jimenez, J., Volkamer, R., Orlando, J., Baidar, S., Brioude, J., Fast, J., Gentner, D., Goldstein, A., et al.: Simulation of semi-explicit mechanisms of SOA formation from glyoxal in aerosol in a 3-D model, Atmosf. Chem. Phys., 14, 6213–6239, https://doi.org/https://doi.org/10.5194/acp-14-6213-2014, 2014.

Knote, C., Hodzic, A., and Jimenez, J.: The effect of dry and wet deposition of condensable vapors on secondary organic aerosols concentrations over the continental US., Atmos. Chem. Phys., 15, https://doi.org/https://doi.org/10.5194/acp-15-1-2015, 2015.

Kota, S. H., Guo, H., Myllyvirta, L., Hu, J., Sahu, S. K., Garaga, R., Ying, Q., Gao, A., Dahiya, S., Wang, Y., et al.: Year-long simulation of gaseous and particulate air pollutants in India, Atmos. Environ., 180, 244–255, https://doi.org/https://doi.org/10.1016/j.atmosenv.2018.03.003, 2018.

Krishna, R. K., Ghude, S. D., Kumar, R., Beig, G., Kulkarni, R., Nivdange, S., and Chate, D.: Surface $PM_{2.5}$ estimate using satellite-derived aerosol optical depth over India, Aerosol Air Qual. Res., 19, 25–37, https://doi.org/https://doi.org/10.4209/aaqr.2017.12.0568, 2019.

Kuik, F., Lauer, A., Churkina, G., Denier van der Gon, H. A., Fenner, D., Mar, K. A., and Butler, T. M.: Air quality modelling in the Berlin–Brandenburg region using WRF-Chem v3. 7.1: sensitivity to resolution of model grid and input data, Geosci. Model Dev., 9, 4339–4363, https://doi.org/https://doi.org/10.5194/gmd-9-4339-2016, 2016.

Kulkarni, S. H., Ghude, S. D., Jena, C., Karumuri, R. K., Sinha, B., Sinha, V., Kumar, R., Soni, V., and Khare, M.: How Much Does Large-Scale Crop Residue Burning Affect the Air Quality in Delhi?, Environ. Sci. Technol., 54, 4790–4799, https://doi.org/https://doi.org/10.1021/acs.est.0c00329, 2020.

Kumar, M., Tiwari, S., Murari, V., Singh, A., and Banerjee, T.: Wintertime characteristics of aerosols at middle Indo-Gangetic Plain: Impacts of regional meteorology and long range transport, Atmos. Environ., 104, 162–175, https://doi.org/https://doi.org/10.1016/j.atmosenv.2015.01.014, 2015a.

Kumar, M., Parmar, K., Kumar, D., Mhawish, A., Broday, D., Mall, R., and Banerjee, T.: Long-term aerosol climatology over Indo-Gangetic Plain: Trend, prediction and potential source fields, Atmos. Environ., 180, 37–50, https://doi.org/https://doi.org/10.1016/j.atmosenv.2018.02.027, 2018.

Kumar, R., Naja, M., Pfister, G., Barth, M., and Brasseur, G.: Simulations over South Asia using the Weather Research and Forecasting model with Chemistry (WRF-Chem): set-up and meteorological evaluation, Geosci. Model Dev., 5, 321–343, https://doi.org/https://doi.org/10.5194/gmd-5-321-2012, 2012a.

Kumar, R., Naja, M., Pfister, G., Barth, M., Wiedinmyer, C., and Brasseur, G.: Simulations over South Asia using the Weather Research and Forecasting model with Chemistry (WRF-Chem): chemistry evaluation and initial results, Geosci. Model Dev., 5, 619, https://doi.org/https://doi.org/10.5194/gmd-5-619-2012, 2012b.

Kumar, R., Barth, M., Pfister, G., Nair, V., Ghude, S. D., and Ojha, N.: What controls the seasonal cycle of black carbon aerosols in India?, J. Geophys. Res.-Atmos., 120, 7788–7812, https://doi.org/https://doi.org/10.1002/2015JD023298, 2015b.

Kusaka, H. and Kimura, F.: Coupling a single-layer urban canopy model with a simple atmospheric model: Impact on urban heat island simulation for an idealized case, J. Meteorol. Soc. Jpn., 82, 67–80, https://doi.org/https://doi.org/10.2151/jmsj.82.67, 2004.

Kuttippurath, J., Singh, A., Dash, S., Mallick, N., Clerbaux, C., Van Damme, M., Clarisse, L., Coheur, P.-F., Raj, S., Abbhishek, K., et al.: Record high levels of atmospheric ammonia over India: Spatial and temporal analyses, Sci. Total Environ., p. 139986, https://doi.org/https://doi.org/10.1016/j.scitotenv.2020.139986, 2020.

Lane, T. E., Donahue, N. M., and Pandis, S. N.: Effect of NO x on secondary organic aerosol concentrations, Environ. Sci. Technol., 42, 6022–6027, https://doi.org/https://doi.org/10.1021/es703225a, 2008a.

Lane, T. E., Donahue, N. M., and Pandis, S. N.: Simulating secondary organic aerosol formation using the volatility basis-set approach in a chemical transport model, Atmos. Environ., 42, 7439–7451, https://doi.org/https://doi.org/10.1016/j.atmosenv.2008.06.026, 2008b.

Lelieveld, J., Bourtsoukidis, E., Brühl, C., Fischer, H., Fuchs, H., Harder, H., Hofzumahaus, A., Holland, F., Marno, D., Neumaier, M., et al.: The South Asian monsoon—pollution pump and purifier, Science, 361, 270–273, https://doi.org/https://doi.org/10.1126/science.aar2501, 2018.

Levy, R., Mattoo, S., Munchak, L., Remer, L., Sayer, A., Patadia, F., and Hsu, N.: The Collection 6 MODIS aerosol products over land and ocean, Atmos. Meas. Tech., 6, 2989, https://doi.org/https://doi.org/10.5194/amt-6-2989-2013, 2013.

Li, J., Georgescu, M., Hyde, P., Mahalov, A., and Moustaoui, M.: Achieving accurate simulations of urban impacts on ozone at high resolution, Environ. Res. Lett., 9, 114 019, https://doi.org/doi:10.1088/1748-9326/9/11/114019, 2014.

Mallik, C. and Lal, S.: Seasonal characteristics of SO 2, NO 2, and CO emissions in and around the Indo-Gangetic Plain, Environ. Monit Assess., 186, 1295–1310, https://doi.org/https://doi.org/10.1007/s10661-013-3458-y, 2014.

Maussion, F., Siller, M., and Rothenberg, D.: fmaussion/salem: v0.2.1, https://doi.org/10.5281/zenodo.3509134, https://doi.org/10.5281/zenodo.269646, 2017.

780 McDuffie, E. E., Smith, S. J., O'Rourke, P., Tibrewal, K., Venkataraman, C., Marais, E. A., Zheng, B., Crippa, M., Brauer, M., and Martin, R. V.: A global anthropogenic emission inventory of atmospheric pollutants from sector-and fuel-specific sources (1970–2017): an application of the Community Emissions Data System (CEDS), Earth Syst. Sci. Data, 12, 3413–3442, https://doi.org/https://doi.org/10.5194/essd-12-3413-2020, 2020.

Met Office: Cartopy: a cartographic python library with a matplotlib interface, Exeter, Devon, http://scitools.org.uk/cartopy, 2010 - 2015.

785 Mhawish, A., Banerjee, T., Sorek-Hamer, M., Bilal, M., Lyapustin, A. I., Chatfield, R., and Broday, D. M.: Estimation of High-Resolution $PM_{2.5}$ over the Indo-Gangetic Plain by Fusion of Satellite Data, Meteorology, and Land Use Variables, Environ. Sci. Technol., 54, 7891–7900, https://doi.org/https://doi.org/10.1021/acs.est.0c01769, 2020.

Ministry of Environment Government of Pakistan: Land Use Atlas of Pakistan, Tech. rep., Government of Pakistan, 2009.

Morrison, H., Curry, J., and Khvorostyanov, V.: A new double-moment microphysics parameterization for application in cloud and climate
790 models. Part I: Description, J. Atmos. Sci., 62, 1665–1677, https://doi.org/https://doi.org/10.1175/JAS3446.1, 2005.

Nakanishi, M. and Niino, H.: An improved Mellor–Yamada level-3 model: Its numerical stability and application to a regional prediction of advection fog, Bound.-Lay. Meteorol., 119, 397–407, https://doi.org/https://doi.org/10.1007/s10546-005-9030-8, 2006.

National Centers for Environmental Prediction, National Weather Service, NOAA, U.S. Department of Commerce: NCEP GDAS/FNL 0.25 Degree Global Tropospheric Analyses and Forecast Grids, https://doi.org/https://doi.org/10.5065/D65Q4T4Z, 2015.

795 Null, J.: El Niño and La Niña years and intensities, https://ggweather.com/enso/oni.htm, last access: 30 November 2020, 2020.

Ojha, N., Sharma, A., Kumar, M., Girach, I., Ansari, T. U., Sharma, S. K., Singh, N., Pozzer, A., and Gunthe, S. S.: On the widespread enhancement in fine particulate matter across the Indo-Gangetic Plain towards winter, Sci. Rep., 10, 1–9, https://doi.org/https://doi.org/10.1038/s41598-020-62710-8, 2020.

OpenAQ: Fighting air inequality through open data and community, https://openaq.org/, last access: 30 November 2020.

800 Pakistan Bureau of Statistics: Provisional Summary Results of 6th Population and Housing Census–2017, Tech. rep., Government of Pakistan Islamabad, 2017.

Pankow, J. F.: An absorption model of gas/particle partitioning of organic compounds in the atmosphere, Atmos. Environ., 28, 185–188, https://doi.org/https://doi.org/10.1016/1352-2310(94)90093-0, 1994.

Pant, P., Shukla, A., Kohl, S. D., Chow, J. C., Watson, J. G., and Harrison, R. M.: Characterization of ambi-
805 ent $PM_{2.5}$ at a pollution hotspot in New Delhi, India and inference of sources, Atmos. Environ., 109, 178–189, https://doi.org/https://doi.org/10.1016/j.atmosenv.2015.02.074, 2015.

Paolella, D. A., Tessum, C. W., Adams, P. J., Apte, J. S., Chambliss, S., Hill, J., Muller, N. Z., and Marshall, J. D.: Effect of model spatial resolution on estimates of fine particulate matter exposure and exposure disparities in the United States, Environ. Sci. Technol. Lett., 5, 436–441, https://doi.org/https://doi.org/10.1021/acs.estlett.8b00279, 2018.

810 Patel, K., Bhandari, S., Gani, S., Campmier, M. J., Kumar, P., Habib, G., Apte, J., and Hildebrandt Ruiz, L.: Sources and Dynamics of Submicron Aerosol during the Autumn Onset of the Air Pollution Season in Delhi, India, ACS Earth Space Chem., 5, 118–128, https://doi.org/https://doi.org/10.1021/acsearthspacechem.0c00340, 2021.

Plotly Technologies Inc.: Collaborative data science, https://plot.ly, 2015.

Rajput, P., Sarin, M., Sharma, D., and Singh, D.: Organic aerosols and inorganic species from post-harvest agricultural-waste burning
815 emissions over northern India: impact on mass absorption efficiency of elemental carbon, Environ. Sci-Proc. Imp., 16, 2371–2379, https://doi.org/https://doi.org/10.1039/c4em00307a, 2014.

Rakesh, V., Singh, R., and Joshi, P. C.: Intercomparison of the performance of MM5/WRF with and without satellite data assimilation in short-range forecast applications over the Indian region, Meteorol. Atmos. Phys., 105, 133–155, https://doi.org/https://doi.org/10.1007/s00703-009-0038-3, 2009.

820 Ram, K., Sarin, M., and Hegde, P.: Atmospheric abundances of primary and secondary carbonaceous species at two high-altitude sites in India: sources and temporal variability, Atmos. Environ., 42, 6785–6796, https://doi.org/https://doi.org/10.1016/j.atmosenv.2008.05.031, 2008.

Ram, K., Sarin, M., and Tripathi, S.: Temporal trends in atmospheric $PM_{2.5}$, $PM_{2.5}$, elemental carbon, organic carbon, water-soluble organic carbon, and optical properties: impact of biomass burning emissions in the Indo-Gangetic Plain, Environ. Sci. Technol., 46, 686–695,
825 https://doi.org/https://doi.org/10.1021/es202857w, 2012.

Ratnam, J. V. and Kumar, K. K.: Sensitivity of the simulated monsoons of 1987 and 1988 to convective parameterization schemes in MM5, J. Climate, 18, 2724–2743, https://doi.org/https://doi.org/10.1175/JCLI3390.1, 2005.

Reddy, C. S., Pasha, S. V., Jha, C., Diwakar, P., and Dadhwal, V.: Development of national database on long-term deforestation (1930–2014) in Bangladesh, Global Planet. Change, 139, 173–182, https://doi.org/https://doi.org/10.1016/j.gloplacha.2016.02.003, 2016.

830 Robinson, A. L., Donahue, N. M., Shrivastava, M. K., Weitkamp, E. A., Sage, A. M., Grieshop, A. P., Lane, T. E., Pierce, J. R., and Pandis, S. N.: Rethinking organic aerosols: Semivolatile emissions and photochemical aging, Science, 315, 1259–1262, https://doi.org/https://doi.org/10.1126/science.1133061, 2007.

Schnell, J. L., Naik, V., Horowitz, L. W., Paulot, F., Mao, J., Ginoux, P., Zhao, M., and Ram, K.: Exploring the relationship between surface $PM_{2.5}$ and meteorology in Northern India, Atmos. Chem. Phys., 18, 10 157–10 175, https://doi.org/https://doi.org/10.5194/acp-18-10157-
835 2018, 2018.

Seinfeld, J. H. and Pandis, S. N.: Atmospheric chemistry and physics: from air pollution to climate change, John Wiley & Sons, 2016.

Sembhi, H., Wooster, M., Zhang, T., Sharma, S., Singh, N., Agarwal, S., Boesch, H., Gupta, S., Misra, A., Tripathi, S. N., Mor, S., and Khaiwal, R.: Post-monsoon air quality degradation across Northern India: assessing the impact of policy-related shifts in timing and amount of crop residue burnt, Environ. Res. Lett., 15, 104 067, https://doi.org/10.1088/1748-9326/aba714, 2020.

840 Shahid, M. Z., Liao, H., Li, J., Shahid, I., Lodhi, A., Mansha, M., et al.: Seasonal variations of aerosols in Pakistan: Contributions of domestic anthropogenic emissions and transboundary transport, Aerosol Air Qual. Res., 15, 1580–1600, https://doi.org/https://doi.org/10.4209/aaqr.2014.12.0332, 2015.

Sharma, A., Ojha, N., Pozzer, A., Mar, K. A., Beig, G., Lelieveld, J., and Gunthe, S. S.: WRF-Chem simulated surface ozone over south Asia during the pre-monsoon: effects of emission inventories and chemical mechanisms, Atmos. Chem. and Phys., 17, 14 393–14 413,
845 https://doi.org/https://doi.org/10.5194/acp-17-14393-2017, 2017.

Sharma, S. and Khare, M.: Simulating ozone concentrations using precursor emission inventories in Delhi–National Capital Region of India, Atmos. Environ., 151, 117–132, https://doi.org/https://doi.org/10.1016/j.atmosenv.2016.12.009, 2017.

Sharma, S., Mandal, T., Srivastava, M., Chatterjee, A., Jain, S., Saxena, M., Singh, B., Sharma, A., Adak, A., Ghosh, S., et al.: Spatio-temporal variation in chemical characteristics of PM 10 over Indo Gangetic Plain of India, Environ. Sci. and Poll. Res., 23, 18 809–18 822,
850 https://doi.org/10.1007/s11356-016-7025-2, 2016.

Shrivastava, M., Cappa, C. D., Fan, J., Goldstein, A. H., Guenther, A. B., Jimenez, J. L., Kuang, C., Laskin, A., Martin, S. T., Ng, N. L., et al.: Recent advances in understanding secondary organic aerosol: Implications for global climate forcing, Rev. Geophys., 55, 509–559, https://doi.org/https://doi.org/10.1002/2016RG000540, 2017.

Singh, A. P., Singh, R., Mina, U., Singh, M. P., and Varshney, C. K.: Emissions of monoterpene from tropical Indian plant species and assessment of VOC emission from the forest of Haryana state, Atmos. Pollut. Res., 2, 72–79, https://doi.org/https://doi.org/10.5094/APR.2011.009, 2011.

Singh, N., Banerjee, T., Raju, M. P., Deboudt, K., Sorek-Hamer, M., Singh, R. S., and Mall, R. K.: Aerosol chemistry, transport, and climatic implications during extreme biomass burning emissions over the Indo-Gangetic Plain., Atmos. Chem. Phys., 18, https://doi.org/https://doi.org/10.5194/acp-18-14197-2018, 2018.

Sirithian, D. and Thepanondh, S.: Influence of grid resolution in modeling of air pollution from open burning, Atmosphere, 7, 93, https://doi.org/https://doi.org/10.3390/atmos7070093, 2016.

Srinivas, B. and Sarin, M.: PM$_{2.5}$, EC and OC in atmospheric outflow from the Indo-Gangetic Plain: Temporal variability and aerosol organic carbon-to-organic mass conversion factor, Sci. Total Environ., 487, 196–205, https://doi.org/https://doi.org/10.1016/j.scitotenv.2014.04.002, 2014.

Stavrakou, T., Müller, J.-F., Bauwens, M., De Smedt, I., Van Roozendael, M., Guenther, A., Wild, M., and Xia, X.: Isoprene emissions over Asia 1979-2012: impact of climate and land-use changes, Atmos. Chem. and Phys., 14, 4587–4605, https://doi.org/https://doi.org/10.5194/acp-14-4587-2014, 2014.

Stibig, H.-J., Belward, A., Roy, P., Rosalina-Wasrin, U., Agrawal, S., Joshi, P., Hildanus, Beuchle, R., Fritz, S., Mubareka, S., et al.: A land-cover map for South and Southeast Asia derived from SPOT-VEGETATION data, JJ. Biogeogr., 34, 625–637, https://doi.org/https://doi.org/10.1111/j.1365-2699.2006.01637.x, 2007.

Stone, E., Schauer, J., Quraishi, T. A., and Mahmood, A.: Chemical characterization and source apportionment of fine and coarse particulate matter in Lahore, Pakistan, Atmos. Environ., 44, 1062–1070, https://doi.org/https://doi.org/10.1016/j.atmosenv.2009.12.015, 2010.

Surl, L., Palmer, P. I., and González Abad, G.: Which processes drive observed variations of HCHO columns over India?, Atmos. Chem. Phys., 18, 4549–4566, https://doi.org/https://doi.org/10.5194/acp-18-4549-2018, 2018.

Tan, J., Zhang, Y., Ma, W., Yu, Q., Wang, J., and Chen, L.: Impact of spatial resolution on air quality simulation: A case study in a highly industrialized area in Shanghai, China, Atmos. Pollut. Res., 6, 322–333, https://doi.org/https://doi.org/10.5094/APR.2015.036, 2015.

The pandas dev. Team: pandas-dev/pandas: Pandas, https://doi.org/10.5281/zenodo.3509134, https://doi.org/10.5281/zenodo.3509134, 2020.

Tie, X., Madronich, S., Walters, S., Zhang, R., Rasch, P., and Collins, W.: Effect of clouds on photolysis and oxidants in the troposphere, J. Geophys. Res.-Atmos., 108, https://doi.org/https://doi.org/10.1029/2003JD003659, 2003.

U.S. Department of State: U.S. Embassy and Consulates' air quality monitors, https://www.airnow.gov/international/us-embassies-and-consulates/, last access: 30 November 2020.

Vadrevu, K. P., Ellicott, E., Badarinath, K., and Vermote, E.: MODIS derived fire characteristics and aerosol optical depth variations during the agricultural residue burning season, north India, Environ. Pollut., 159, 1560–1569, https://doi.org/https://doi.org/10.1016/j.envpol.2011.03.001, 2011.

Venkataraman, C., Brauer, M., Tibrewal, K., Sadavarte, P., Ma, Q., Cohen, A., Chaliyakunnel, S., Frostad, J., Klimont, Z., Martin, R. V., et al.: Source influence on emission pathways and ambient PM$_{2.5}$ pollution over India (2015–2050), Atmos. Chem. Phys., 18, 8017–8039, https://doi.org/https://doi.org/10.5194/acp-18-8017-2018, 2018.

Wang, T., Song, Y., Xu, Z., Liu, M., Xu, T., Liao, W., Yin, L., Cai, X., Kang, L., Zhang, H., et al.: Why is the Indo-Gangetic Plain the region with the largest NH 3 column in the globe during pre-monsoon and monsoon seasons?, Atmos. Chem. Phys., 20, 8727–8736, https://doi.org/https://doi.org/10.5194/acp-20-8727-2020, 2020.

WHO: Ambient air pollution: A global assessment of exposure and burden of disease, Tech. rep., World Health Organization, WHO, 2016.

Wiedinmyer, C., Akagi, S., Yokelson, R. J., Emmons, L., Al-Saadi, J., Orlando, J., and Soja, A.: The Fire INventory from NCAR (FINN): a high resolution global model to estimate the emissions from open burning, Geosci. Model Dev., 4, 625, https://doi.org/https://doi.org/10.5194/gmd-4-625-2011, 2011.

895 Zaveri, R. A., Easter, R. C., Fast, J. D., and Peters, L. K.: Model for simulating aerosol interactions and chemistry (MOSAIC), J. Geophys. Res.-Atmos., 113, https://doi.org/https://doi.org/10.1029/2007JD008782, 2008.

Zhang, M., Uno, I., Zhang, R., Han, Z., Wang, Z., and Pu, Y.: Evaluation of the Models-3 Community Multi-scale Air Quality (CMAQ) modeling system with observations obtained during the TRACE-P experiment: Comparison of ozone and its related species, Atmos. Environ., 40, 4874–4882, https://doi.org/https://doi.org/10.1002/2017JD027057, 2006.

900 Zhang, Q., Beekmann, M., Drewnick, F., Freutel, F., Schneider, J., Crippa, M., Prevot, A. S., Baltensperger, U., Poulain, L., Wiedensohler, A., et al.: Formation of organic aerosol in the Paris region during the MEGAPOLI summer campaign: evaluation of the volatility-basis-set approach within the CHIMERE model, Atmos. Chem. Phys., 13, 5767–5790, https://doi.org/https://doi.org/10.5194/acp-13-5767-2013, 2013.

Zhang, R., Lei, W., Tie, X., and Hess, P.: Industrial emissions cause extreme urban ozone diurnal variability, P. Natl. Acad. Sci. USA, 101, 905 6346–6350, https://doi.org/https://doi.org/10.1073/pnas.0401484101, 2004.

Zhao, B., Wang, S., Donahue, N. M., Jathar, S. H., Huang, X., Wu, W., Hao, J., and Robinson, A. L.: Quantifying the effect of organic aerosol aging and intermediate-volatility emissions on regional-scale aerosol pollution in China, Sci. Rep., 6, 28 815, https://doi.org/https://doi.org/10.1038/srep28815, 2016.